A study on fully nonlinear wave load effects on floating wind turbine

Kun Xu [a,*], Yanlin Shao [b,c], Zhen Gao [a,d,e], Torgeir Moan [a,d,e]

[a] Department of Marine Technology, Norwegian University of Science and Technology (NTNU), Trondheim 7491, Norway
[b] Department of Mechanical Engineering, Technical University of Denmark, 2800 kgs., Lyngby, Denmark
[c] Shipbuilding Engineering Institute, Harbin Engineering University, 150001 Harbin, China
[d] Centre for Ships and Ocean Structures (CESOS), NTNU, Trondheim 7491, Norway
[e] Centre for Autonomous Marine Operations and Systems (AMOS), NTNU, Trondheim 7491, Norway

ARTICLE INFO

ABSTRACT

The influence of fully nonlinear wave effects on floating wind turbine has been studied in this paper by comparing both floater motions and structural responses of tower base and mooring lines exposed to linear and fully nonlinear long-crested irregular waves. Wave kinematics of the linear and nonlinear wave are calculated in a 2D Harmonic Polynomial Cell wave tank. The wave kinematics are further processed by a polynomial fitting method to scale down the data size so that it fulfills the memory requirement of HAWC2 where coupled dynamic analysis is carried out. The external DLL used to provide wave kinematics to HAWC2 is extended from one dimensional (Wkin.dll 2.4) to two dimensional (Wkin.dll 2D) wave field so that fully nonlinear wave can be implemented on floating wind turbine through reading pre-generated wave kinematics manner. The whole work procedure including wave generation, polynomial fitting and implementation in HAWC2 has been verified with a linear regular wave case. Two extreme irregular wave conditions are focused to study the nonlinear wave effects regarding critical responses, such as wave elevation, floater motions and mooring line tension. The results have not only proved the accuracy and applicability of the polynomial fitting method and the extended Wkin.dll 2D for HAWC2 but also revealed the importance to consider fully nonlinear wave model in hydrodynamic analysis compared with linear wave theory especially for high sea states in shallow and intermediate water. As a result of development of computer capacity and numerical wave tank, this paper has demonstrated that fully nonlinear wave effect can be considered in an engineering manner with acceptable efficiency.

1. Introduction

As floating wind turbines become more and more competitive in offshore wind energy market, the hydrodynamic behavior of floating structure in intermediate water depths (50 m–200 m) has drawn a lot of attention especially regarding the effect of the wave nonlinearity. The widely used linear Airy wave is mainly suitable for small wave in deep water and cannot provide accurate results for large wave in shallow water. The stream function wave model can capture most of the important nonlinearities. However, it does not work for irregular nonlinear waves, thus is less useful in practice

---

when irregular waves are concerned. Larger extreme loads and load effects are expected in the case of fully nonlinear wave model in particular for extreme environmental conditions, in which wind turbine blades are parked and wave loads dominate over wind loads. It is therefore necessary to consider fully nonlinear wave in hydrodynamic analysis in order to calculate the wave loads and the structural responses of floating wind turbines properly.

Fully nonlinear wave interaction with submerged structures was investigated by Bai et al. (2014) using a three-dimensional numerical wave tank based on potential theory. The higher-order boundary element method is used to solve the mixed boundary value problem. Schløer et al. (2011) studied the effect of fully nonlinear irregular unidirectional wave acting on a monopile. Inline force and overturning moment resulted from nonlinear waves was found to be significantly larger than from linear wave. In some cases, stream function theory underestimates the wave forces compared with fully nonlinear irregular wave. The aeroelastic code used to model the wind turbine is FLEX5 Øye (1996) and the undisturbed fully nonlinear wave kinematics was obtained from OceanWave3D which is a fully nonlinear potential wave model proposed by Engsig-Karup et al. (2009) from DTU. OceanWave3D is able to solve 3D Laplace equation for the velocity potential with nonlinear free surface boundary conditions (FSBC). Schløer et al. (2012) performed comparative analysis regarding the fatigue damage of the monopile and tower due to fully nonlinear irregular wave. Fatigue damage level was seen to be significantly affected by nonlinear wave especially for misaligned wave and wind condition. In Schløer et al. (2016), linear and nonlinear wave realization were looked into detail. Redistribution of energy at different frequency range was observed from wave spectrum. The largest positive wave peaks come from nonlinear wave realization for all the condition compared with linear wave, so does the largest skewness. The difference between linear and nonlinear results increases with decreasing water depth due to increasing wave nonlinearity for reduced water depth. Nonlinear wave effects was also investigated for jacket supported wind turbine by Larsen et al. (2011). Significant increase in dynamic load effect due to nonlinear wave was found for tower bottom bending moment and axial force in both right leg and lower X-brace.

Despite all the previous work on bottom fixed wind turbine, there has been limited similar research work on floating wind turbines. Computational fluid dynamics (CFD) method has been used to study the fully nonlinear wave effect on a TLP floating wind turbine by Nematbakhsh et al. (2015). The results was compared with results from potential flow solver − Simo-Riflex. However, aerodynamic load was not included, nor does aeroelastic response of the wind turbine due to high computational cost. The coupled FLEX5-OceanWave3D tool was applied on a TLP wind turbine in the INNWIND project (Bredmose, 2013) to compare response exposed to different wave models including fully nonlinear wave. The result was further compared with experimental data in Pegalajar-Jurado et al. (2017). Pegalajar-Jurado et al. (2017) concluded that it was quite difficult to determine which wave model included was the most accurate because the wave models with different sets of wave kinematics cannot provide consistent prediction. Therefore, it is more challenging to apply fully nonlinear wave on floating wind turbine than bottom fixed wind turbine in terms of accuracy and efficiency. One of the reasons is that the footprint of floating wind turbines is larger due to its mooring system which requires larger database for pre-generated wave kinematics in the whole wave field to be used in a global response analysis. Normally the database is so large that it exceeds the virtual memory limit of the simulation tool for wind turbine. Therefore, there is a need to scale down the data size to meet the requirement at the first place. In addition, it is so demanding to obtain accurate fully nonlinear wave kinematics due to complicated fully nonlinear FSBCs that a separate numerical wave tank (NWT) is needed to generate the wave. Build a link between the wave kinematics database and the simulation tool is also quite important.

The main objective of this paper is to study fully nonlinear wave effect on a semi-submersible floating wind turbine. The fully nonlinear waves are generated in a 2D numerical wave tank based on the Harmonic Polynomial Cell method which is an efficient field solver. The coupled dynamic analysis is carried out in HAWC2. In accordance to the first memory boundary challenge, a polynomial fitting method is proposed in order to decrease the data size. The wave kinematics at pre-defined grid points in the whole wave field is fitted to polynomial functions representing location coordinates and corresponding polynomial coefficients. The method is verified against HAWC2 default wave. The other contribution of this paper is extending the dynamic link library between wave kinematics database and HAWC2 from one dimensional to two dimensional so that it can be applied not only on bottom fixed wind turbine but also on floating wind turbine. The hydrodynamic wave load in HAWC2 is calculated using Morison's equation. The nonlinear effect considered in this paper mainly includes nonlinear wave kinematics generated from a numerical wave tank; hydrodynamic load calculation for the floater up to the instantaneous free surface of the incident waves, geometrical nonlinearity for mooring line. A regular wave case is performed for verification and two extreme irregular wave conditions are compared for the nonlinear effects. Wave kinematics, wave spectrum, floater motion, tower base force and mooring line tension are compared.

2. Wave theory

Ocean wave is a random and irregular process whose mathematical formulations can be determined based on several boundary conditions on water surface and sea bottom. Wave theories can be divided into linear and nonlinear groups according to the simplification level of boundary conditions. A linear regular wave has a sinusoidal surface profile with small amplitude and steepness, while a nonlinear wave has sharper crests and flatter troughs. The nonlinear regular waves can be described by Stokes, cnoidal, stream function or solitary wave theories according to the nonlinear properties of the waves. The applicability of various wave theories is discussed in DNV-RP-C205 DNVGL (2017) as shown in Fig. 1.
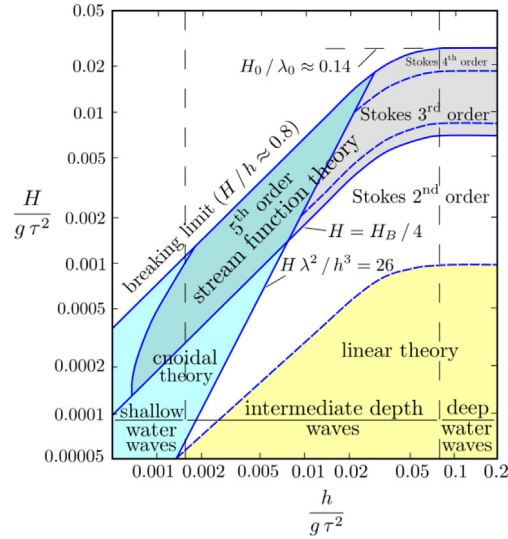
Fig. 1. Applicability of various wave theories.

Horizontal axis is a non-dimensional measurement of depth shallowness and the vertical axis is a measurement of wave steepness.

The nonlinearity of a large transient wave event can be described by higher order bound and resonant nonlinearities (Gibson and Swan, 2006). Bound nonlinearities are induced by higher order nonlinear harmonics which are phase locked to the first order wave component. They tend to modify the free surface profile by sharping the peaks and flattening the troughs. Resonant nonlinearities on the other hand influences the energy distribution within the wave spectrum by adjusting the phases and amplitudes of the first order wave components and produces new wave components satisfying dispersion relation.

2.1. Linear wave theory

Linear wave theory also known as Airy wave theory is the most widely used wave theory in offshore industry. It is based on the assumption that the contribution from the nonlinear terms in FSBCs are negligible. The mathematical expression can be derived considering a incompressible, inviscid and irrotational fluid.

1. Laplace equation is the governing equation in the fluid domain:

$$\nabla^2 \phi = 0 \tag{1}$$

2. Considering wave elevation, η which is proportional to wave height H is small, the FSBCs can be linearized and described at the still water level (SWL) $z = 0$ instead of $z = \eta$ using Taylor's expansion. Dynamic FSBC is written as:

$$\frac{\partial \phi}{\partial t} = -g\eta \quad \text{on} \quad z = 0 \tag{2}$$

where the atmospheric pressure is assumed to be zero on the free surface.

3. Kinematic FSBC is expressed as

$$\frac{\partial \eta}{\partial t} = \frac{\partial \phi}{\partial z} \quad \text{on} \quad z = 0 \tag{3}$$

4. The impermeability condition, such as sea bottom and fixed body surfaces is described as:

$$\frac{\partial \phi}{\partial n} = 0 \tag{4}$$

2.2. Fully nonlinear wave theory

Linear wave theory is formulated on the basis that only the linear terms are kept in FSBCs while nonlinear terms are totally neglected. It can provide good estimation of the wave kinematics for small waves in deep water (water depth is larger than half of the wavelength). However, the contribution from nonlinear terms becomes significant when water depth is small. Therefore, fully nonlinear wave theory is a better option. The different FSBCs are written as:

- Fully nonlinear dynamic FSBC

$$\frac{\partial \phi}{\partial t} = -g\eta - \frac{1}{2} \bigtriangledown \phi \cdot \bigtriangledown \phi \qquad \text{on} \qquad z = \eta(x, y) \tag{5}$$

- Fully nonlinear kinematic FSBC

$$\frac{\partial \eta}{\partial t} = \frac{\partial \phi}{\partial z} - \overline{\bigtriangledown}\phi \cdot \overline{\bigtriangledown}\eta \qquad \text{on} \qquad z = \eta(x, y) \tag{6}$$

Here $\bigtriangledown = \vec{i}\frac{\partial}{\partial x} + \vec{j}\frac{\partial}{\partial y} + \vec{k}\frac{\partial}{\partial z}$ and $\overline{\bigtriangledown} = \vec{i}\frac{\partial}{\partial x} + \vec{j}\frac{\partial}{\partial y}$. $\vec{i}, \vec{j}$ and $\vec{k}$ are unit vectors along x-, y- and z-axis respectively.

When a material derivative following an arbitrary velocity $\vec{v} = \{v_x, v_y, v_z\}$ is introduced, the fully nonlinear FSBCs can be rewritten as:

$$\frac{D\phi}{Dt} = -g\eta - \frac{1}{2} \bigtriangledown \phi \cdot \bigtriangledown \phi + \vec{v} \cdot \bigtriangledown \phi \qquad \text{on} \qquad z = \eta(x, y) \tag{7}$$

$$\frac{D\eta}{Dt} = \frac{\partial \phi}{\partial z} - \overline{\bigtriangledown}\phi \cdot \overline{\bigtriangledown}\eta + \{v_x, v_y\}^T \cdot \overline{\bigtriangledown}\eta \qquad \text{on} \qquad z = \eta(x, y) \tag{8}$$

In this paper, a semi-Lagrangian approach will be used by following the vertical velocities of fluid particles on the free surface, which means in 2D case the following FSBCs shall be applied in the numerical implementation:

$$\frac{D\phi}{Dt} = -g\eta - \frac{1}{2} \bigtriangledown \phi \cdot \bigtriangledown \phi + \frac{\partial \phi}{\partial z}(\frac{\partial \phi}{\partial z} - \frac{\partial \phi}{\partial x}\frac{\partial \eta}{\partial x}) - \mu(x)\phi \qquad \text{on} \qquad z = \eta(x, y) \tag{9}$$

$$\frac{D\eta}{Dt} = \frac{\partial \phi}{\partial z} - \overline{\bigtriangledown}\phi \cdot \overline{\bigtriangledown}\eta + \{v_x, v_y\}^T \cdot \overline{\bigtriangledown}\eta - \mu(x)\phi \qquad \text{on} \qquad z = \eta(x, y) \tag{10}$$

Here $\mu(x)$ is a damping coefficient to dissipate the energy of the waves which exists only in the damping zone at the end of the numerical wave tank.

3. Hydrodynamic load modeling

Potential flow theory and Morison's equation are the two typical methods for hydrodynamic load calculation of floating wind turbine in global analysis. Computational Fluid Dynamics (CFD) has become more popular in recent years as well thanks to the rapid development of computer capacity. Matha et al. (2011) has discussed the advantages and limitations of all three methods.

3.1. Morison's equation

Morison's equation which is used in this paper is a semi-empirical method to calculate the wave loads on slender structures whose diameter-to-wavelength ratio is less than 1/5. The diffraction and radiation effects are considered not significant. It has been mostly applied on slender vertical surface-piercing cylinders such as monopile and spar. Some recent research results also proved the applicability for small-diameter floating wind turbine like semi-submersible in high sea states compared to model scale measurements (Robertson et al., 2013).

The hydrodynamic loading according to Morison's equation is expressed in terms of the undisturbed fluid-particle velocity and accelerations directly which allows Morison's equation to be applied in the case of nonlinear wave and current kinematics models (Santo et al., 2018).

The wave force dF on a strip of length dz of a rigid moving circular cylinder can be written as:

$$dF = \rho \frac{\pi D^2}{4} dz C_M a_n + \rho \frac{\pi D^2}{4} dz (C_M - 1)a_c + \frac{\rho}{2} C_D D dz |u_{rel}| u_{n,rel} \tag{11}$$

where D is the cylinder diameter, a_n is the undisturbed wave induced acceleration components normal to the cylinder axis, a_c is the normal component of cylinder acceleration, $u_{n,rel}$ is the component of the relative velocity normal to the cylinder, C_M and C_D are the mass and drag coefficients which are dependent of several parameters such as Reynolds number, the roughness number and the Keulegan–Carpenter number. The coefficients should be determined empirically and C_M can be determined according to the result from potential flow theory.

One advantage of Morison's equation is the hydrodynamic load calculation is based on undisturbed fluid particle velocity and acceleration instead of velocity potential which is expressed with frequency-dependent added mass, damping and wave excitation force. As a result, Morison's equation provides a more straightforward manner to consider nonlinear wave or current kinematics models. Accordingly in this paper, Morison's equation is used to carry out the hydrodynamic load calculation.

3.2. Radiation/diffraction theory

As the size of supporting floating substructure increases, wave diffraction and radiation effects become more significant and cannot inherently be captured by Morison's equation. In such case, potential flow theory is preferred. The first order potential problem solves diffraction and radiation problems separately with linearized boundary value problems whose solution is frequency-dependent and linearly related with wave amplitude. Added mass, damping and restoring matrices and incident wave excitation from diffraction are pre-computed in frequency domain. Viscosity is incorporated through drag term of the Morison's equation. Difference frequency and sum frequency effects are considered by second order potential theory which are important for slow drift motion of semi-submersible and ringing of TLP. Second order hydrodynamic effects can be obtained by either full quadratic transfer functions (QTF) which take into account the contribution from all six degrees of freedom or Newman's approximation which only requires the diagonal terms of the full QTF matrix while the off-diagonal terms are approximated by the diagonal terms for the two directions and periods involved. The frequency domain results are applied in time domain simulation through Cummins equation (Cummins, 1962). Take a floating single degree-of-freedom system including mooring system and viscous drag force as an example, the motion equation in time domain can be written as:

$$(M + A_\infty)\ddot{x}(t) + \int_{-\infty}^{+\infty} \kappa(t - \tau)\dot{x}(\tau)d\tau + Cx(t) + K(x(t)) = F^{FK} + F^D + C_q |u - \dot{x}| (u - \dot{x}) \tag{12}$$

where M is the mass of the body, A_∞ is the added mass at infinity frequency, $\kappa(t-\tau)$ is the retardation function consisting of frequency-dependent added mass and damping coefficient, C is the hydrostatic restoring force, $K(x(t))$ is the nonlinear restoring force from the mooring system, F^{FK} is the Froude–Krylov force, F^D stands for the diffraction force, the quadratic damping force is related to the relative velocity between body velocity and fluid particle velocity.

3.3. Computational fluid dynamics

Computational fluid dynamics (CFD) method can include all relevant linear and nonlinear hydrodynamic effects including viscous effects. Normally, finite-volume method is used to solve the Reynolds-Averaged Navier–Stokes (RANS) equations on grids while free surface can be represented by the volume of fluid (VOF) approach (Carrión et al., 2014). Viscous effects are included to describe vortex separation at mooring line and floater. Despite the accuracy in hydrodynamic wave modeling, high computational effort is expected which still requires a lot of effort before engineering application. Meanwhile, current CFD studies are restricted to wave-only simulation and it is challenging to include aerodynamic effects at the same time.

4. Harmonic polynomial cell method

4.1. 2D HPC method

The numerical wave tank used in this paper to generate fully nonlinear wave is based on 2D harmonic polynomial cell (HPC) method which was initially proposed by Shao and Faltinsen (2012) as a potential flow solver with approximately 4th order accuracy. The highlight of HPC method is that the fluid domain is divided into quadrilateral cells associated with harmonic polynomials which are used to describe the velocity potential in each cell. It has been compared with four other methods and demonstrates great efficiency and accuracy. The HPC method was developed to 3D case by Shao and Faltinsen (2014b), and implemented in fully-nonlinear wave body interaction problems such as sloshing in 3D tanks, shallow water wave tank, influence from seabed topography and nonlinear wave diffraction by a bottom-mounted vertical circular cylinder. Promising results again proved the applicability of HPC method when dealing with potential flow problems. Later on, the current effects was studied together with nonlinear wave diffraction by multiple bottom mounted cylinder in Shao and Faltinsen (2014a). Improvement of HPC method was made by Liang et al. (2015) in order to account for singular flows and discontinuous problems. Domain decomposition method combining with local potential flow solution was proposed to handle the singularity at sharp corners. A double-layer node technique is developed to model the velocity potential jump in a thin free shear layer in lifting problem.

Brief introduction of HPC method is given here while detailed theory can be referred to Shao and Faltinsen (2012, 2014a,b). According to 2D HPC method, the fluid domain is discretized into quadrilateral cells within which there are four quadrilateral elements and nine grid nodes as shown in Fig. 2. The stencil center is located in the middle node with index 9 while eight other nodes are boundary nodes numbering from 1 to 8. The velocity potential ϕ within the cell is expressed by harmonic polynomials which automatically satisfy Laplace equation. Therefore, the velocity potential at any point in the cell can be interpolated by a linear combination of the eight harmonic polynomials at the surrounding boundary nodes.

$$\phi(x, y) = \sum_{j=1}^{8} b_j f_j(x, y) \tag{13}$$

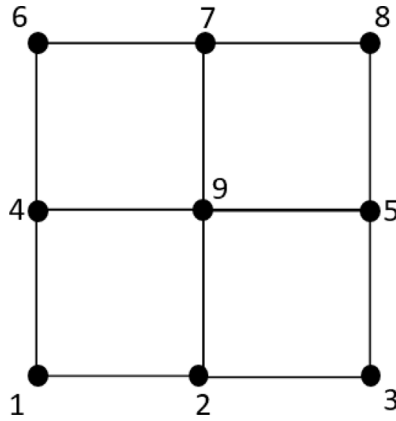**Fig. 2.** Grid node indexes in a cell.

Where $f_1(x, y) = 1$; $f_2(x, y) = x$; $f_3(x, y) = y$; $f_4(x, y) = x^2 - y^2$; $f_5(x, y) = xy$; $f_6(x, y) = x^3 - 3xy^2$; $f_7(x, y) = 3x^2y - y^3$; $f_8(x, y) = x^4 - 6x^2y^2 + y^4$

Including higher order polynomials could reduce the wave dispersion errors in the time domain analysis and increase the accuracy of the solution.

The way to calculate the unknown coefficients b_j term is equivalent to a sub-Dirichlet boundary value problem with Laplace equation as the governing equation. Combining $x = x_j$, $y = y_j$, $\phi = \phi_j$ with Eq. (13), a linear equation with a precise form is achieved:

$$b_i = \sum_{j=1}^{8} c_{i,j}\phi_j \quad (i = 1, \ldots, 8) \tag{14}$$

here $c_{i,j}(i, j = 1, \ldots, 8)$ is the elements of the inverse of matrix $[D]$ which consists of elements $d_{i,j} = f_j(x_i, y_i)$. Therefore, the velocity potential at any grid point in the fluid domain could be described based on the eight surrounding boundary nodes in the same stencil cell. Considering the stencil center where $x = x_9 = 0$ and $y = y_9 = 0$, the resulting harmonic polynomials is expressed as $f_1(0, 0) = 1$ and $f_j(0, 0) = 0, j = 2, \ldots, 8$. Accordingly, the velocity potential at the cell center is described as:

$$\phi_9 = \phi(x = x_9 = 0, y = y_9 = 0) = \sum_{i=1}^{8} c_{1,i}\phi_i \tag{15}$$

The Dirichlet boundary condition is related to velocity potential at the boundary nodes, while the Neumann boundary condition is enforced by taking the normal derivative:

$$\frac{\partial \phi}{\partial n}(x, y) = \sum_{i=1}^{8} \left[\sum_{j=1}^{8} c_{j,i} \nabla f_j(x, y) \cdot n(x, y) \right] \phi_i \tag{16}$$

where n is the normal vector, defined as positive pointing outside of the fluid domain.

4.2. Time integration, wave generation and wave absorption

An explicit 4th order Runge–Kutta method is applied to integrate Eqs. (9) and (10) in time to update the wave elevation and velocity potential on the free surface. Auxiliary solutions at three time instants are needed in the 4-stage time integration. For each time step, four solutions of the boundary value problem for the velocity potential in the whole fluid domain are obtained by the HPC method, which has been described in Section 4.1.

Wavemaker at left end of the numerical wave tank is used to generate the target waves. It is known that a sudden start of a wavemaker will introduce instability and breakdown of the simulation eventually. Thus, a ramp function $r(t)$ is applied to the wavemaker signal $s(t)$ so that the modified signal becomes $s(t) = \bar{s}(t) \cdot r(t)$. In this study, the following ramp function is applied

$$r(t) = \begin{cases} \frac{1}{2}[1 - \cos(\pi \frac{t}{T_{ramp}})], & t < T_{ramp} \\ 1, & t \geq T_{ramp} \end{cases} \tag{17}$$

Here T_{ramp} is the duration of the ramp, which is taken as 2 times of the peak period T_p of the wave spectrum.
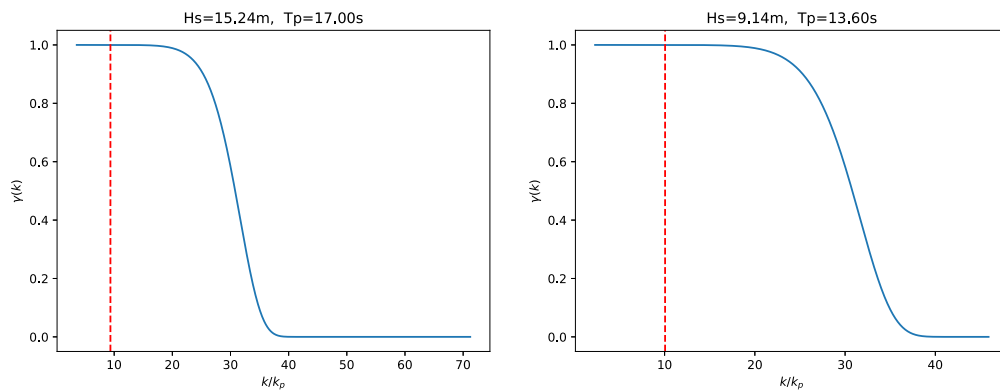
Fig. 3. Filter strength.

A numerical damping zone is implemented at the end of the numerical wave tank to dissipate the energy of the waves. A quadratic function, which has been suggested by Ning and Teng (2007) is applied:

$$\mu(x) = \begin{cases} \mu_0(\frac{x-x_b}{\lambda_b})^2, & x > x_b \\ 0, & x \le x_b \end{cases} \tag{18}$$

Here x is the coordinate measured from the location of the wavemaker. x_b is the location where the damping zone starts and λ_b is the length of the damping zone. The length of the damping zone and the damping strength μ_0 are so chosen to minimize the wave reflection from the wall at the end of the tank.

It is necessary to apply a free-surface filter in order to simulate nonlinear steep waves over a long time duration without any instability developing. Without such a filter, sawtooth instability will eventually occur for waves over a certain steepness as consequence of aliasing effects due to the quadratic terms in fully nonlinear free surface conditions. In this study, the simulated wave elevation along the numerical wave tank is projected into wavenumber space through FFT technique, and the following filter is then applied to the resulting wave numbers

$$\gamma(k) = exp(-(\frac{k}{\alpha \cdot k_0})^\beta) \tag{19}$$

Here k_0 is a reference wave number, which normally corresponds to a characteristic wave number of the considered wave spectrum. In this study, k_0 is taken as k_p, which is the root of the dispersion relationship $\omega_p^2 = k_p h \cdot \tanh(k_p h)$. Here $\omega_p = 2\pi/T_p$. h is the water depth. α and β are constant coefficients.

An ideal filter should be able to sufficiently remove energy from very short waves while keep the important waves unchanged. α and β are determined through $\gamma(k_{max}) = 0.01$ and $\gamma(k_{min}) = 0.99$ which indicate that the filter takes away 99% wave amplitude from a short wave with wave number k_{max} and only 1% wave amplitude from a wave with wave number k_{min}. In this study, $k_{max} = 2\pi/(4\Delta x)$ and $k_{min} = 2\pi/(10\Delta x)$ are used in all the analysis with irregular waves. Δx is the size of the element along horizontal direction of the numerical wave tank. Since the filter strength is dependent on the discretization and the characteristic wave number $k_0 = k_p$, it is important to understand the effect of the filter before generating the nonlinear irregular waves.

Fig. 3 is an example of the filter strength $\gamma(k)$ as function of k/k_p for a sea state with $H_s = 15.24$ m and $T_p = 17.0$ s to the left and $H_s = 9.14$ m and $T_p = 13.6$ s to the right. The horizontal discretization is defined with $\Delta x = \frac{\lambda_p}{40} = \frac{2\pi}{k_p} \cdot \frac{1}{40}$, which means that 40 elements are uniformly distributed within a characteristic wave length, which corresponds to the peak-frequency of the spectrum. According to Fig. 3, the filter completely removes energy for waves with $k/k_p \ge 40$ while it has almost no effect for waves with $k/k_p \le 20$.

When a wave spectrum is used to generate irregular waves in the time domain, it is common practice to truncate the wave spectrum by a lower-limit frequency ω_l and upper-limit frequency ω_u. The cut-off frequency limit in this paper is determined mainly based on two aspects: the important waves containing most of the energy cannot be cut off and extremely short wave which requires quite fine mesh should be cut off in order to avoid numerical breakdown and increase of CPU time. As recommended in Stansberg et al. (2008) and DNVGL (2017), the cut-off limit defined in this paper is: $\omega_u = \sqrt{2g/H_s}$ and $\omega_l = 0.4 * \omega_p$, which leads to only 0.9% and 1.1% loss of the zero-th moments of the wave spectra for ULS1 and ULS2 condition respectively. The vertical dashed lines in Fig. 4 represent the cut-off frequencies while the red lines represent the wave spectra.

At the same time, the vertical lines in Fig. 3 indicate the wave number corresponding to the upper-limit truncation frequency ω_u. It is quite obvious that the applied filter has negligible effects on the important waves that should be simulated through the truncated wave spectrum. If a finer mesh is used, the filter will have even less effects on the waves that are of practical interests in the studies presented in this paper.
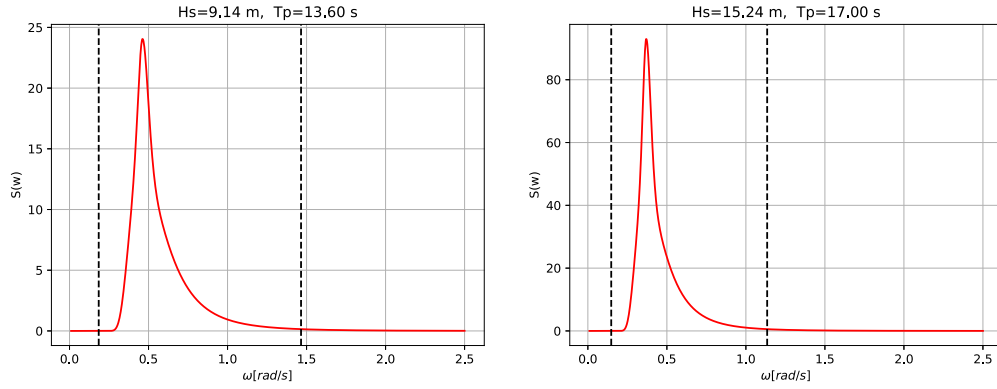
Fig. 4. Cut-off of wave spectra for ULS1 and ULS2 condition.
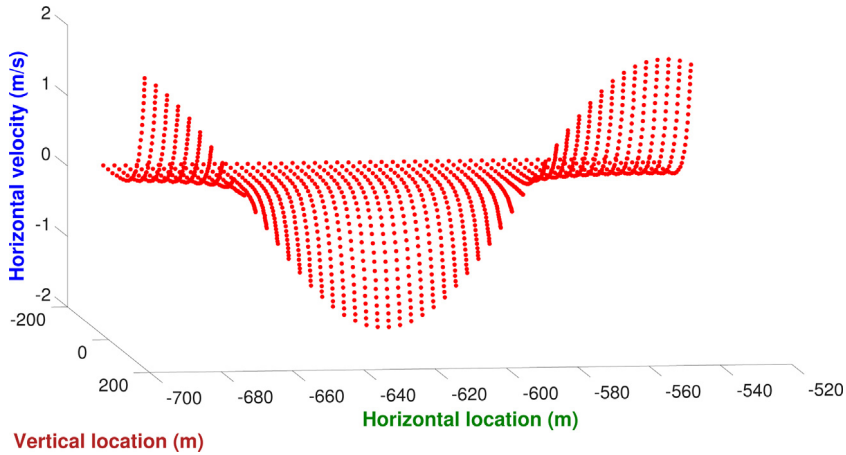

Fig. 5. Horizontal velocity at 200 s.

4.3. Polynomial fitting of wave kinematics

The velocity potential, wave elevation, velocity are directly calculated from 2D HPC wave tank, while acceleration is available by post-processing velocity and grid deformation. All the grids are fixed in the tank in linear wave making problem, while the grids deform vertically in nonlinear case which leads to the difference when calculating the acceleration. Bernoulli's equation is only valid in an inertial system. Therefore, material derivative is introduced to calculate the acceleration (Faltinsen and Timokha, 2009):

$$\frac{\partial U}{\partial t} = \frac{\delta U}{\delta t} - w_{grid} \cdot \nabla U \tag{20}$$

Since the grid deformation only appears in vertical direction, Eq. (20) can be further written as:

$$\frac{\partial U}{\partial t} = \frac{\delta U}{\delta t} - \frac{\partial z}{\partial t} \cdot \frac{\partial U}{\partial z} \tag{21}$$

Where U is the velocity, $\frac{\partial z}{\partial t}$ is the relative velocity representing the grid deformation in vertical direction.

The wave kinematics data obtained from the wave tank at each time step is expressed at discrete grid points across the whole wave field. Fig. 5 is an example of the horizontal velocity of wave particles in the wave field with corresponding horizontal and vertical coordinates at a certain time step. At the same time step, there are three other similar figures representing vertical velocity, horizontal acceleration and vertical acceleration which are not shown here. It takes about 18 h to calculate a 1 h irregular wave realization with 148 grids horizontally and 22 grids vertically in a normal computer when only 2 processors are engaged. However, the size of resulting wave kinematics files including wave elevation, velocity and acceleration in both horizontal and vertical directions is around 8 GB, which exceeds the memory requirement of the simulation tool for wind turbine, HAWC2 in this study. Besides, huge occupation of virtual memory will slow down the computation especially for floating wind turbine whose element number is normally very large. Therefore, there is an urgent need to scale down the size of input wave data.

Table 1
Polynomial function.

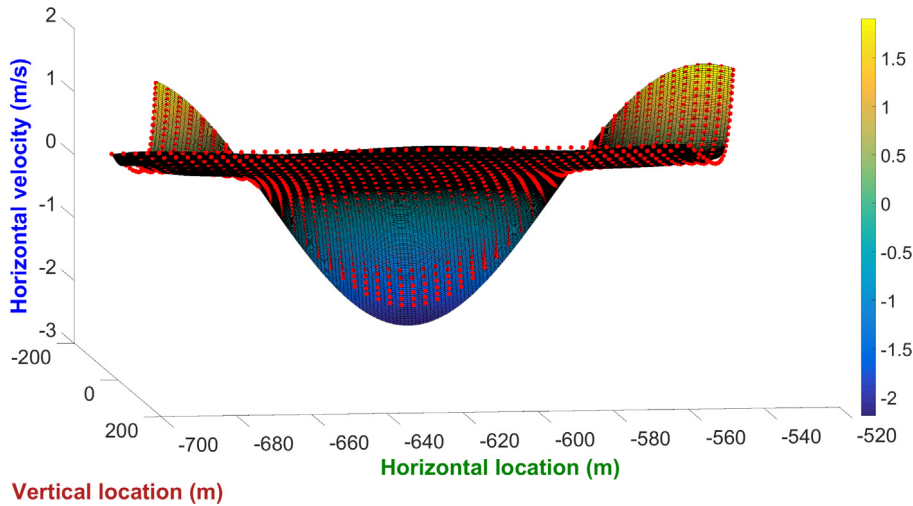| Order	Polynomial
0	1
1	xz
2	$x^2 xz z^2$
3	$x^3 x^2 z x z^2 z^3$
…	…
n	$x^n x^{n-1} z x^{n-2} z^2 \quad \ldots \quad x^2 z^{n-2} x z^{n-1} z^n$

Fig. 6. Fitting surface and original data.

In accordance to the challenge, a polynomial fitting method is presented. First of all, the vertical and horizontal dimensions of the wave field are determined by water depth and footprint of the mooring system respectively. Normally, it is sufficient to use 50 grids horizontally per wavelength and 30 grids along water depth. Then the whole wave field is divided into a number of horizontal divisions based on the wavelength. The kinematics varies at both horizontal and vertical directions.

Therefore within each division, a 2 dimensional polynomial function representing horizontal and vertical coordinates up to a certain order n is introduced as shown in Table 1. The corresponding coefficients using least-squares method are calculated and arranged in a descending power regarding x coordinate. As a result, the kinematics data at each time step can be expressed in a function form instead with location coordinates as input variables:

$$U = c_1 x^n + c_2 x^{n-1} z + \cdots + c_{\frac{(n+1)(n+2)}{2}-2} xz^{n-1} + c_{\frac{(n+1)(n+2)}{2}-1} z^n + c_{\frac{(n+1)(n+2)}{2}} \tag{22}$$

Here x represents horizontal coordinate, z represents vertical coordinate and c_i is corresponding polynomial coefficient.

In nonlinear wave problem, the vertical coordinates of the grid points can be directly applied as input for z, since the grids deform vertically following instantaneous wave elevation up to the free surface. Meanwhile, in linear wave problem, the grid is fixed and the kinematics is calculated below mean water level. Therefore, Wheeler stretching method is applied to obtain the kinematics up to the free surface by scaling vertical coordinate:

$$z' = (z - \eta)\frac{d}{d + \eta} \tag{23}$$

Where z is original grid coordinate, z' is scaled coordinate, η is the instantaneous free surface elevation and d is water depth.

As a result, the wave kinematics at any locations in the whole wave field at each time step can be calculated based on Eq. (22), which include not only the original grid points directly from the wave tank as shown in Fig. 5 but also at the locations between the grid points. The resulting wave kinematics information can be expressed with a fitting surface where different color represent different amplitude of the kinematics. Fig. 6 is an example of the fitting surface for horizontal velocity and it can be seen that the velocity between the grid points are available as well represented by the fitting surface. The same procedure is applied to acceleration and velocity in both horizontal and vertical directions.

In the end, the original wave kinematics expressed at discrete grid points are replaced by coefficients c_i and corresponding polynomial functions x_i, z_i representing horizontal and vertical coordinates. The size of data is decreased
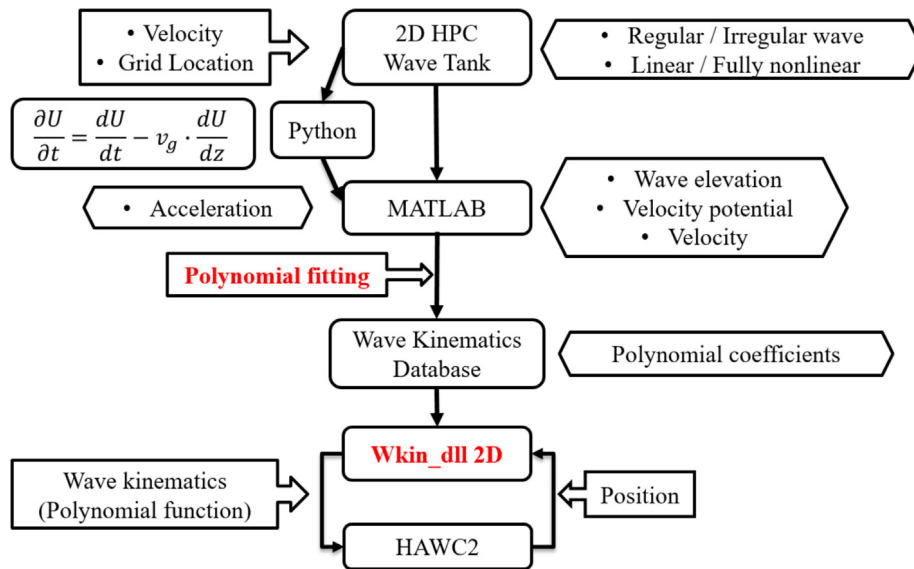
Fig. 7. Work flow.

from 8 GB to 1 GB for a 1 h irregular wave problem using 148 grids horizontally and 22 grids vertically, which fulfills the memory requirement of HAWC2 and can be imported through reading pre-generated wave kinematics manner. The order of the polynomial function applied should be carefully chosen in order to achieve good result especially for irregular wave problems whose variation of wave kinematics is harder to predict.

5. Methodology

5.1. Work flow

The main focus of this paper is to study the fully nonlinear wave effects on floating wind turbine using 2D HPC wave tank and HAWC2 with extended Wkin.dll 2D to handle wave kinematics polynomial coefficients. The work procedure is demonstrated in Fig. 7. The contribution of this paper are marked with red color.

1. Step1: 2D HPC numerical wave tank is first used to generate regular or irregular wave with linear or fully nonlinear FSBCs. Wave elevation, velocity and velocity potential are directly available from the tank while the acceleration is obtained through post-processing based on information of velocity and grid location. The calculation of acceleration is based on Eq. (21) and performed in Python.
2. Step2: A Matlab code package based on polynomial fitting method Eq. (22) is developed and applied to fit wave velocity and acceleration data to polynomial coefficients and store as a wave kinematics database.
3. Step3: Finally the coupled dynamic time domain analysis based on Morison's equation is carried out in HAWC2 and the wave kinematics at required location is calculated through Wkin.dll 2D using location coordinates sent from HAWC2 and polynomial coefficients sent from wave kinematics database.

5.2. Modeling theory

HAWC2 (Horizontal Axis Wind turbine simulation Code 2nd generation) is an aeroelastic code developed at DTU Wind Energy in 2003–2006. It is intended for calculating the response of offshore floating and fixed wind turbines in the time domain Larsen and Hansen (2007).

In HAWC2, multibody formulation is the basis of the structural modeling strategy meaning that the wind turbine is divided into several bodies and each body is modeled using a number of Timoshenko beam elements. The coupling constraints connecting individual bodies make it possible to account for the nonlinear structural effects due to body rotation or deformation.

The aerodynamic modeling is based on blade element momentum theory (BEM) and was extended by Hansen et al. (2004) to include dynamic stall, skew inflow and operation in sheared inflow etc. Turbulent inflow can be generated using Mann model and potential flow method is applied to describe tower shadow effects. Control of the turbine is achieved through several DLLs.
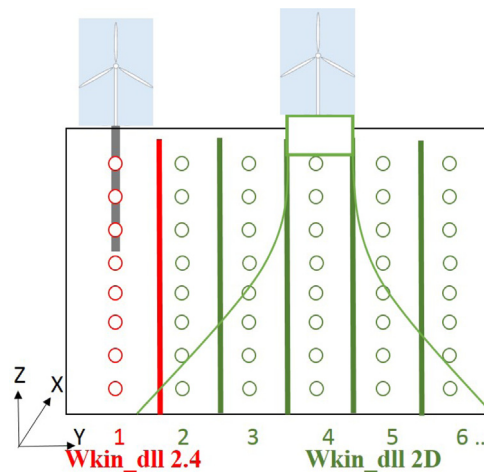
Fig. 8. Wave field structure of wkin.dll in HAWC2.

One option of the hydrodynamic modeling in HAWC2 is based on potential flow theory coupling with output results from WAMIT (Borg et al., 2016) for large volume structures to account for diffraction effect. The other alternative is Morison's equation suitable for small-diameter structures. Buoyancy loads are included through integration of external pressure contribution and inserted as concentrated forces on end nodes and distributed forces over conical sections.

Mooring lines for floating wind turbine can be modeled in either a quasi-static or dynamic manner (Kim et al., 2013). Quasi-static mooring line model is based on pre-calculated results from MIMOSA where stiffness property is described using fairlead position against restoring forces from mooring line. In each time step, the mooring line tension is iterated according to the configuration of each mooring line with the assumption that each mooring line is in static equilibrium at the moment. Inertial effects and damping of the mooring system from wave, current are neglected in quasi-static model (Jonkman, 2009). Dynamic mooring line model was developed by Kallesøe and Hansen (2011) using a cable element with hydrodynamic drag and buoyancy forces. The bottom contact is modeled by a nonlinear spring stiffness. The stiffness of each element is influenced by deflection and orientation of the element. The formulation is applicable for cables with uniform properties so that sections with different cable types are modeled separately and connected by ball joint constraints. Clump weight and buoy can be included as point mass with linear and quadratic viscous damping terms. In this paper, dynamic mooring line model is applied to account for the dynamic effect.

5.3. Wave kinematics (Wkin.dll)

The wave kinematics applied in HAWC2 are provided externally through a defined DLL interface named Wkin.dll. In the current version Wkin.dll 2.4, the input wave types can be selected from: linear airy waves with Wheeler stretching; irregular Airy waves based on JONSWAP or PM spectrum with directional spreading; stream function wave and pre-generated wave kinematics.

When importing pre-generated wave kinematics, the wave field that Wkin.dll 2.4 is able to handle can be considered as a one dimensional field since the data are imported at discrete grid points at only one horizontal location along the water depth as the red part in Fig. 8. The wave kinematics variation only exists in one dimension. The kinematics at any point and the wave elevation are linearly interpolated using the neighboring points. This works sufficiently for bottom fixed wind turbine such as monopile where only the wave kinematics at the center of the structure is needed since the movement of monopile is very small.

However, it is not applicable for floating wind turbine where the variation along horizontal direction is needed as well due to the mooring system. Therefore, the Wkin.dll is further extended in this paper to include wave kinematics variation in horizontal direction in order to implement on floating wind turbine (green part in Fig. 8). It is named Wkin.dll 2D because it is able to handle wave field in two dimensions. Wave elevation is linearly interpolated at different horizontal locations. The wave kinematics including velocity and acceleration are first calculated in numerical wave tank and then fit into polynomial coefficients to scale down the size as introduced in Section 4.3. Wkin.dll 2D will receive the location coordinates sent from HAWC2 and delivers the exact wave kinematics value using the polynomial fitting method. The wave loads on both floater and mooring line are calculated based on Morison's equation.

The extension of the wave field from one dimensional to two dimensional makes it possible to perform hydrodynamic analysis for floating wind turbine using pre-generated wave kinematics method, which is the basis for fully nonlinear wave effect study.
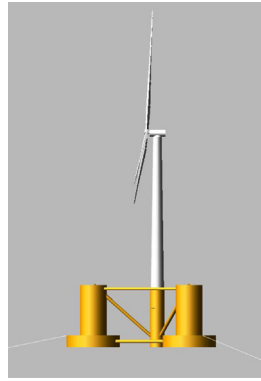
Fig. 9. OC4 semi-submersible wind turbine (Robertson et al., 2014a).

Table 2
Load cases.

	Type	H or Hs [m]	T or Tp [s]	Simulation time [s]	Time step [s]	No. of runs
REG	Regular	6	10	700	0.02	1
ULS1	Irregular	9.14	13.6	4200	0.02	20
ULS2	Irregular	15.24	17	4200	0.02	20

6. Case study

6.1. OC4 semi-submersible floating wind turbine

The floating wind turbine studied in this paper is 5MW OC4 semi-submersible wind turbine as shown in Fig. 9. The floater includes a center column connecting the tower and three side columns which is connected with main column through a number of smaller pontoons and braces (Robertson et al., 2014a). The design is aiming for 200 m water depth with 20 m draft. Three catenary mooring lines are arranged symmetrically about the platform vertical axis with 120° angle between them. The radius from the floater center is 40.87 m to fairlead and 837.6 m to anchor. Unstretched length of all three mooring lines is 835.5 m with 0.0776 m diameter and 108.63 kg/m apparent mass in fluid per unit length. The detailed layout and structural property is available in Robertson et al. (2014a).

Coupled dynamic analysis has been performed through a code comparison involving 23 organizations and 19 simulation tools (Robertson et al., 2014b) to study the structural behavior under different environmental conditions using different modeling philosophies. 23 load cases consisting of standstill frequency analysis without wind and wave loads; standstill case with wave loads; fully coupled dynamic analysis with both wind and wave loads were analyzed. Fully nonlinear wave effects has not been included. At the same time, potential flow theory and Morison's equation are also compared regarding hydrodynamic modeling. Diffraction effects are important to consider using potential flow theory when the structure diameter is larger than 0.2 times wavelength. The results from the comparison is that as for the main structures and pre-defined sea states, the diameter to wavelength ratio calculated only exceeds 0.2 for some lowest sea states, where hydrodynamic loads are small anyway. For the high sea states involved, Morison's equation is able to provide equally accurate results as potential flow theory. A detailed comparison is available in Robertson et al. (2014b). In this paper, Morison's equation is applied for hydrodynamic modeling in HAWC2 while mooring line is represented with dynamic model. The hydrodynamic load on the floater is calculated by integrating the force up to the free surface. The force acting on the mooring line is also calculated based on Morison's equation.

6.2. Load cases

It is important to check beforehand that whether the polynomial fitting method is able to provide reliable results compared with current available code with respect to predicting wave kinematics and responses e.g. floater motion and mooring line tension. Accordingly, a wave-only linear regular wave case is first performed to verify the polynomial fitting method. Afterwards, two irregular wave-only cases representing extreme sea states are considered to study the effect due to fully nonlinear wave.

The sea states selected in this paper is based on the pre-defined condition as listed in Robertson et al. (2014b) and the metocean data at Norway 5 site in North sea (Li et al., 2015). Water depth considered is 200 m. A regular wave condition is selected for verification as a representative case labeled as *REG* in Table 2. Polynomial fitting method is compared with default input wave from HAWC2 as a reference. Regular wave verification simulation is run for 700 s and the system

Table 3
Nonlinear effect.

	Linear wave	Fully nonlinear wave
Nonlinear wave kinematics	Not included	Included
Instantaneous water level	Included	Included
Nonlinear mooring line	Included	Included
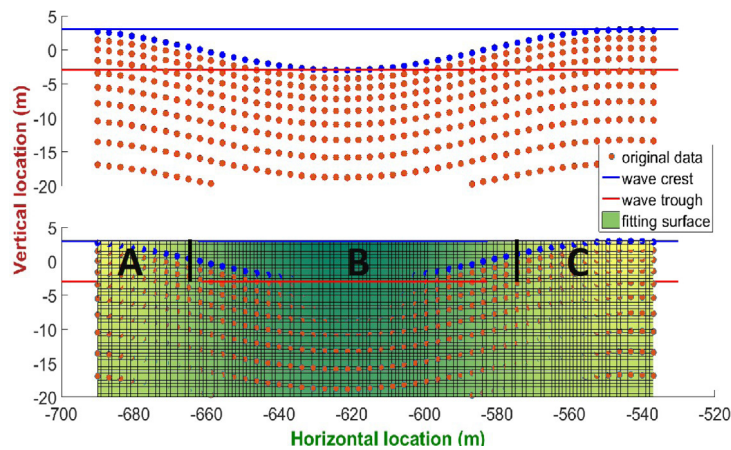
Fig. 10. Location coordinates of the grid points and fitting surface. (For interpretation of the references to color in this figure legend, the reader is referred to the web version of this article.)

becomes stable after 200 s. Only the results from 400 s to 450 s are presented in the following section due to the similarity. The two ultimate-limit-state (ULS) irregular wave conditions are based on JONSWAP spectrum. In each ULS condition, 20 simulations of linear and fully nonlinear wave are performed respectively and same random seed is used for the two wave models within each simulation so that the wave generated follows the same trend but with different amplitude. The total length of the simulation is 4200 s while first 600 s is removed due to transient effect. The following result is taken as the average of 20 simulation results to account for stochastic uncertainty as much as possible. In the following tables and figures, the notation of *HAWC2-Linear* stands for the results using default linear wave from HAWC2 while notation of *HPC-Linear* stands for the results using the new method — polynomial fitting kinematics from HPC wave tank. *Linear* and *Nonlinear* represent waves generated using linear and fully nonlinear FSBCs respectively.

The main objective of this paper is to study the nonlinear effect due to wave. Therefore, all the other nonlinear effects involved in the modeling are kept the same for the two models including calculation of hydrodynamic load up to instantaneous water level and nonlinearity in the mooring line model. The only difference is the nonlinear effect in wave kinematics as shown in Table 3.

6.3. Verification of the analysis procedure

The verification of the proposed analysis procedure (using 2D HPC method, polynomial fitting method and Wkin.dll 2D) for linear wave case against pure HAWC2 analysis is considered with respect to wave kinematics obtained from fitting function compared with original data; wave kinematics observed from HAWC2 simulation; floater motion and mooring line tension predicted using polynomial fitting method and default wave.

6.3.1. Wave kinematics
The polynomial fitting results are checked in the following section regarding how well it represents original data and predicts wave kinematics at other locations in the field. Meanwhile, the output from HAWC2 simulation is also compared between the new method and default regular wave.

Wave kinematics data is fit to polynomial coefficients after being generated fromt the 2D HPC numerical wave tank. Fig. 10 shows the location coordinates of original grid points whose vertical coordinates follows the wave elevation and the resulting fitting surface. It can be considered as the top view of original data (Fig. 5) and fitting surface (Fig. 6) where only the location coordinates are shown without the actual kinematics value. Fig. 11 is the cross-section of the fitting surface (Fig. 6) at wave crest and wave trough. It is used as an example to judge whether fitting surface can coincide with original data at different water depth from free surface to seabed.

Since the vertical coordinates of the data points have been Wheeler stretched using Eq. (23), all the data points follow the instantaneous wave elevation in vertical direction. Therefore in Fig. 10, the original data at free surface (blue dots) are not located at exact wave crest level (blue line) or wave trough level (red line) but at different levels in between.
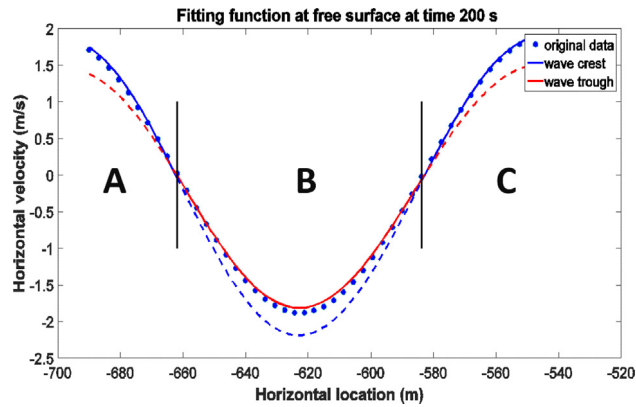
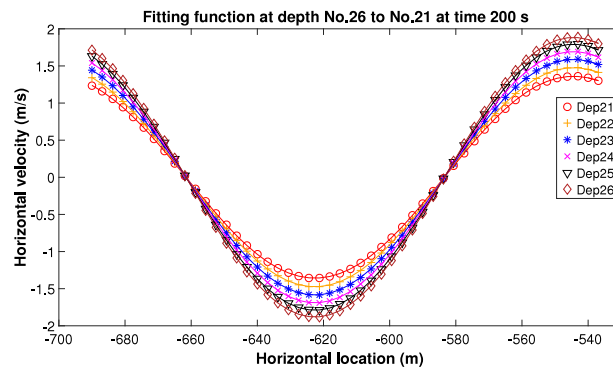**Fig. 11.** Cross-section of the fitting surface at free surface.

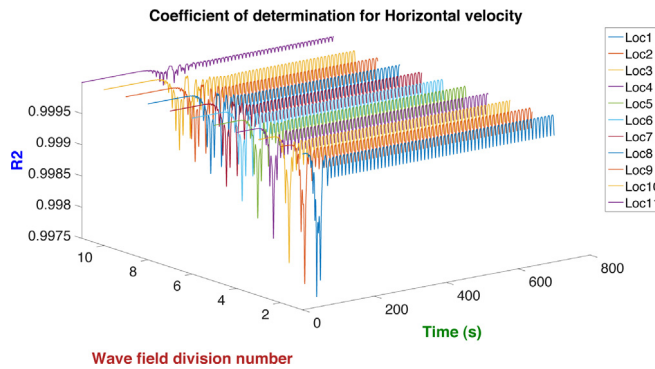**Fig. 12.** Fitting function along various water depths.

Fig. 13. Coefficient of determination.

The cross section of the fitting surface (Fig. 6) at wave crest and wave trough level do not go through all the free surface points (blue dots) exactly since the vertical coordinates are different as shown in Fig. 10, but it will provide an indication about how close original and predicted data are when their coordinates are close. Accordingly, original data is compared with wave crest level (blue solid line) in region A and C and wave trough level (red solid line) in region B considering close vertical coordinates. In Fig. 11, the dashed part of fitting curves are not used for comparison because they are less close to original data by contrast. It is observed that the fitting curves (solid part) predict quite close to original data. It is safe to conclude that the coincidence will be even better when the cross section at exact coordinate as the data is used.

The fitting result is checked at several other different water depths in Fig. 12. The two parts of each fitting line are determined based on the same principle as Fig. 11: the maximum and minimum vertical coordinate at that depth level. Different colors and markers are used to distinguish different water depths.
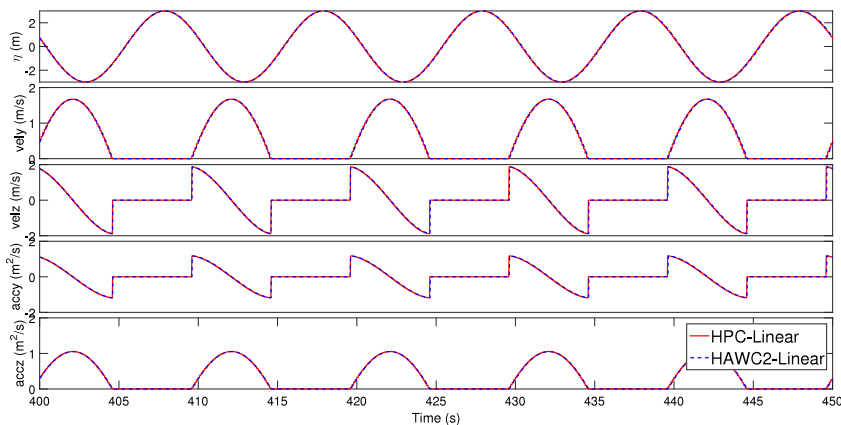
Fig. 14. Wave kinematics at (0 m, 0 m, 0 m). (For interpretation of the references to color in this figure legend, the reader is referred to the web version of this article.)

From statistical point of view, coefficient of determination, denoted R^2 is a measure of how well predicted model has represented original data.

$$R^2 = 1 - \frac{\sum_i (y_i - f_i)^2}{\sum_i (y_i - \bar{y})^2} \tag{24}$$

Where y_i is original data, f_i is predicted data and $\bar{y}$ is the mean of original data. The closer R^2 is to 1, the better linear regression results fit original data. R^2 are calculated for all the wave field divisions at each time step in Fig. 13, as the wave is slowly generated to steady state after 200 s, R^2 becomes stationary with minimum value being 0.9993 for all the divisions, which indicates that the fitting surface provides great representation of original data.

The wave-only regular wave dynamic analysis is performed using the polynomial fitting method and compared with default regular wave in HAWC2. The wave kinematics output of the simulation are also checked. Since HAWC2 is a 2D simulation tool, both velocity and acceleration in x direction are negligible. The wave kinematics observed at location (0 m, 0 m, 0 m) are shown in Fig. 14 including wave elevation; horizontal and vertical velocity; horizontal and vertical acceleration.

The blue line is the results calculated using default wave in HAWC2 while the red line is obtained from polynomial fitting method. Wave elevation from HPC method is linearly interpolated using data at nearest two discrete grid points while result from HAWC2 default wave is calculated based on the analytical expression. The kinematics at the observed point is only non-zero below instantaneous free surface, therefore it drops to zero when free surface goes below the point which is between 0 m and 3 m in Fig. 14 (the positive z direction in HAWC2 points downwards towards seabed). The prediction from the two methods is so close to hardly distinguish from the figure.

The wave kinematics decay along water depths which is captured in Fig. 15 where the data at three depths below free surface are plotted. There is almost no difference between the two methods. In conclusion, HPC polynomial fitting method is able to calculate wave kinematics correctly.

6.3.2. Floater motion

Surge, heave and pitch responses are shown in Fig. 16. Surge response will oscillate about zero-mean position if Morison's equation is calculated at the undisplaced position of the body without wave stretching. However, there should be a slight non-zero drift surge motion in reality. The phenomenon can be captured as illustrated in Fig. 16 when Morison's equation is integrated up to the instantaneous wave elevation using a stretching method. Meanwhile, the buoyancy force in HAWC2 is calculated by integrating static pressure over the bottom and conical sections of the structure with additional contribution from Archimedes method which only includes the normal component to the structure. Therefore, the FK term in the Morison's equation is used by HAWC2 to represent the dynamic pressure integration in the transverse direction (Karimirad et al., 2011). Heave and pitch motion oscillate about zero mean position while HPC method predicts slightly larger heave motion than HAWC2. The difference is due to the error during the polynomial fitting of the wave kinematics using HPC method and the fitting error is more obvious in vertical direction whose kinematics variation is large. However, the heave and pitch response prediction is not significantly affected considering the total response and can be accepted.

6.3.3. Mooring line tension

Mooring line 2 is in the upwind direction oriented with zero wind wave incoming direction while line 1 and 3 are symmetric in the downwind direction. The mean tension and maximum tension are pretty close predicted by the two
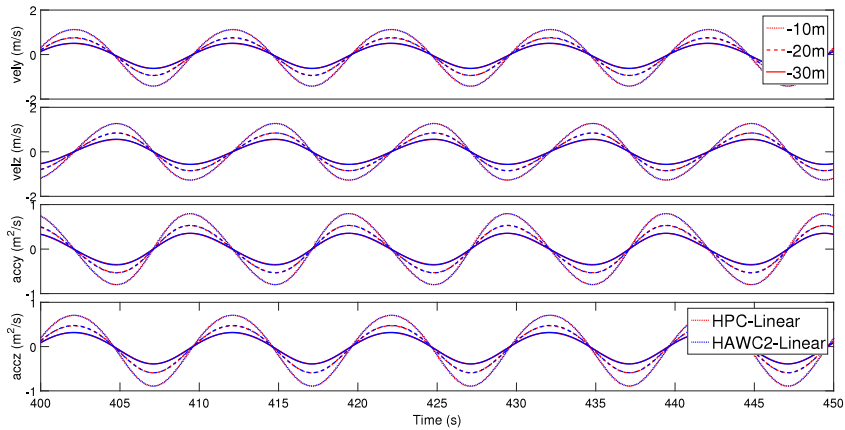
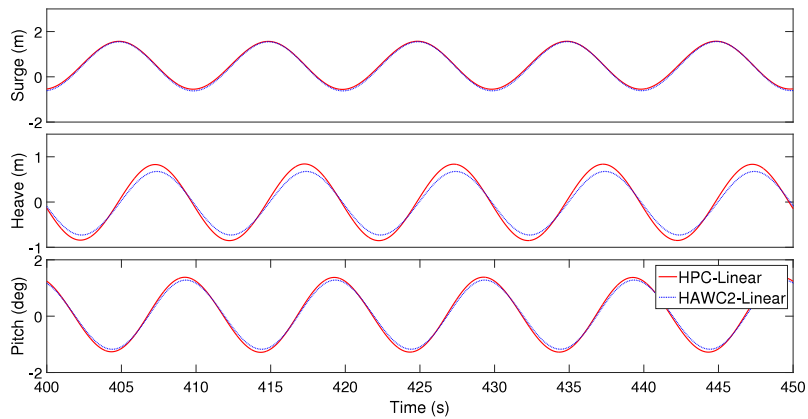**Fig. 15.** Wave kinematics along different water depths.
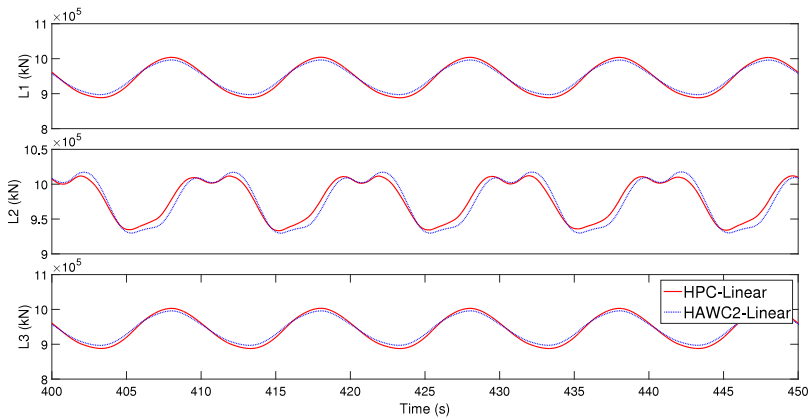

Fig. 16. Motion response.

Fig. 17. Mooring line tension.

methods. The two continuing peak detected in mooring line 2 is due to the excitation of mooring line from the wave, which is captured by the dynamic mooring modeling method. If a quasi-static modeling method is applied, only one peak will be found (Robertson et al., 2014b).

In conclusion, wave kinematics from new proposed HPC polynomial fitting method not only saves the data size but also keeps the accuracy at a high level. The corresponding motion and tension response are also predicted correctly (see Fig. 17).
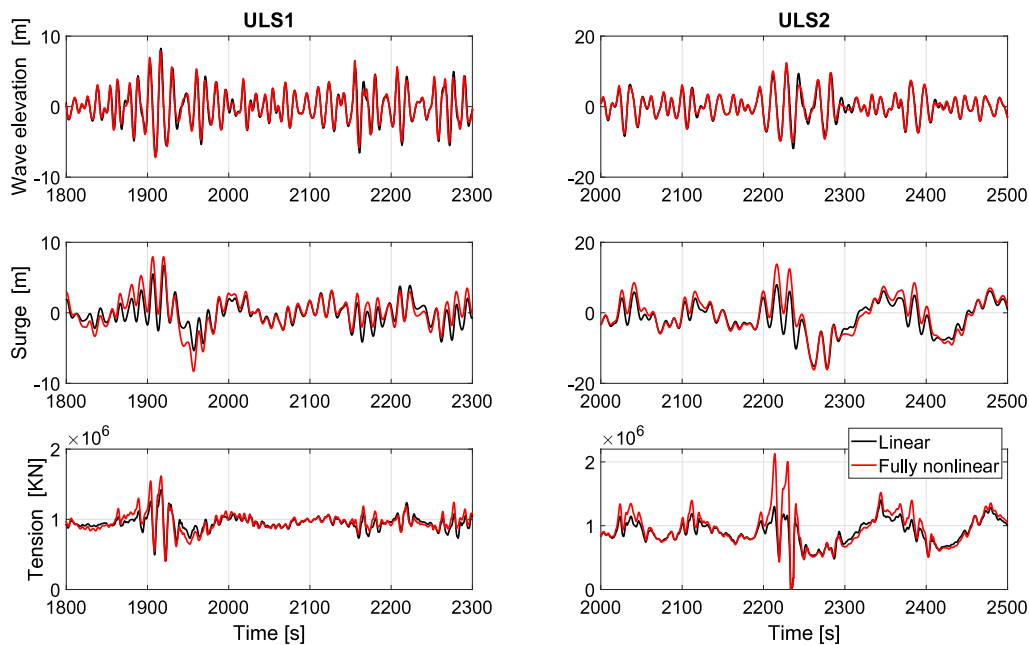
Fig. 18. Time series.

6.4. Irregular wave

The previous regular wave case has proved the accuracy and applicability of the polynomial fitting method. In the following section, the two irregular sea states are compared based on results from 20 simulations. The sea states are defined in Table 2. Both linear and fully nonlinear analysis are run for 4200 s while first 600 s is removed in order to get results for one hour simulation. The following figures and statistics are based on all the 20 simulation results. Fig. 18 is an example of time series for wave elevation, floater surge motion and mooring line tension in the two conditions. Black line represents results due to linear wave and red line represents results due to fully nonlinear wave.

6.4.1. Global maxima

Since the same seed number is used to generate the wave for linear and fully nonlinear wave , the time series of the wave and response follow the same trend just with different amplitudes. The peak amplitude illustrates the difference between the two wave models, which is the basis of the statistical study of this paper. From statistical point of view, probability of exceeding a given threshold by an random maximum provides direct indication of the distribution of maximum response and it can be fit with asymptotic extreme value probability distribution model when the number of sample is large enough. Accordingly, the occurrence probability of a certain level of response can be then predicted. The probability of exceedance is calculated as:

$$P(X_i) = 1 - \frac{i}{N+1} \tag{25}$$

Where X_i is the response sorted in an increasing order. N is the total number of peaks.

Normally, global response maxima of a stationary Gaussian narrow-band process can be well modeled by a Rayleigh distribution (Fu et al., 2017). However, when non-Gaussian and nonlinear property of the process increases, in order to get an accurate expression of the upper tail distribution, Weibull distribution is preferred instead of Rayleigh distribution. In this paper, the largest maximum response between adjacent zero-up-crossing above the mean response level is selected as the global response maxima. Fig. 19 is an example of the global maxima selection of the wave elevation. Blue line is the realization of the wave elevation and green line is the level of mean value and the red dots represent the selected global maxima. The exceedance probability above 0.1 is fitted with Rayleigh distribution while the tail part with probability below 0.1 is decided to be fitted with Weibull distribution. The global maxima of the responses with exceedance probability level of 10^{-4} for the fitted probability function are extrapolated and marked as extreme 10^{-4} in the following tables, which are mainly used to give a direct comparison of the two wave models. In the following section, results of linear and nonlinear wave from ULS1 and ULS2 conditions are shown together with different colors and markers. The fitting probability distribution are plotted using dashed line with the same color as the original maxima data. The horizontal axis represents the global maxima of the response and the vertical axis representing the probability of exceedance is expressed in a logarithmic scale for better representation.
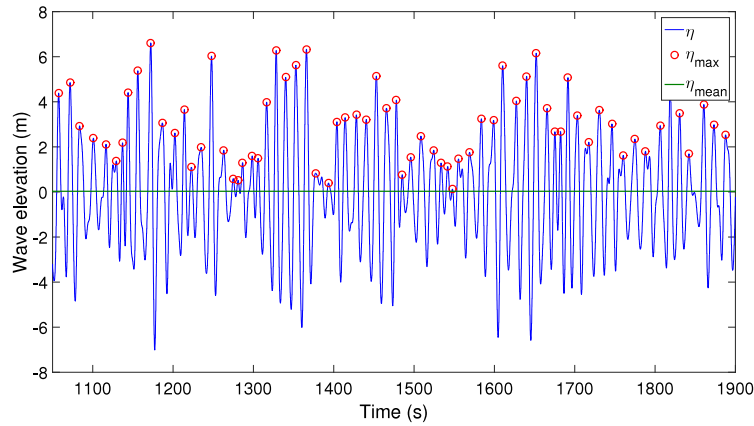
Fig. 19. Selection of global maxima of the wave elevation. (For interpretation of the references to color in this figure legend, the reader is referred to the web version of this article.)
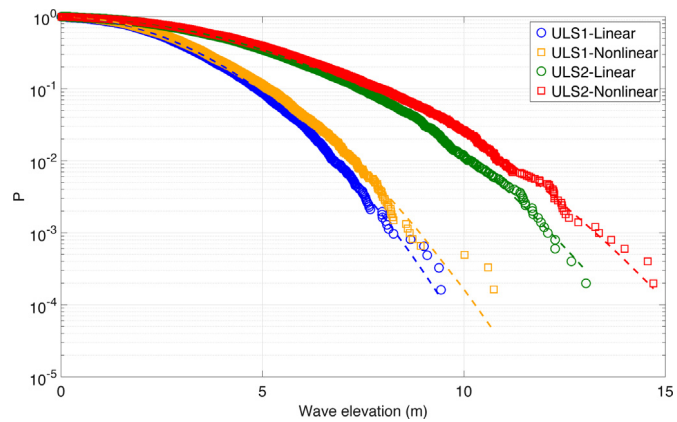

Fig. 20. Global maxima of positive wave peaks at (0 m, 0 m, 0 m).

Table 4
Statistics of wave elevation.

	ULS1 linear	ULS1 nonlinear	ULS2 linear	ULS2 nonlinear
Mean [m]	9.79e−5	6.27e−4	3.55e−4	7.36e−3
Maximum [m]	7.85	8.67	11.3	12.2
Standard deviation [m]	2.24	2.23	3.43	3.40
Skewness	0.00287	0.120	0.00883	0.170
Kurtosis	3.02	3.05	2.90	2.94
Extreme 10^{-4} [m]	9.79	10.60	13.78	15.59

6.4.2. Wave realization

The property of the wave observed at location (0 m, 0 m, 0 m) is first compared with time realization and wave spectrum.

Fig. 20 shows the probability of exceedance for positive wave peaks observed at (0 m, 0 m, 0 m) obtained from linear and nonlinear wave in two conditions. The peaks are selected according to the definition of global maxima in Eq. (25). In general, distinction is not obvious between linear and nonlinear curves at probability level larger than 0.1 for smaller wave peaks. It is mainly the higher maxima with probability level below 0.1 that has clear difference. Higher peaks are predicted from nonlinear wave than linear wave and the difference is more obvious in higher sea state (ULS2). When the same exceedance probability is considered, fully nonlinear wave tends to predict higher value. The mixed Rayleigh–Weibull distributions is able to predict the probability of the original data quite well.

Maximum elevation, skewness and kurtosis of wave elevation taken as the average of all 20 simulations are presented in Table 4. Nonlinear wave in general predicts larger maximum elevations than linear wave for both cases, which is mainly due to the additional contribution from the nonlinear terms. The standard deviations calculated for the linear and fully nonlinear wave are quite close with slightly higher value for linear wave, indicating that linear wave contains a bit higher
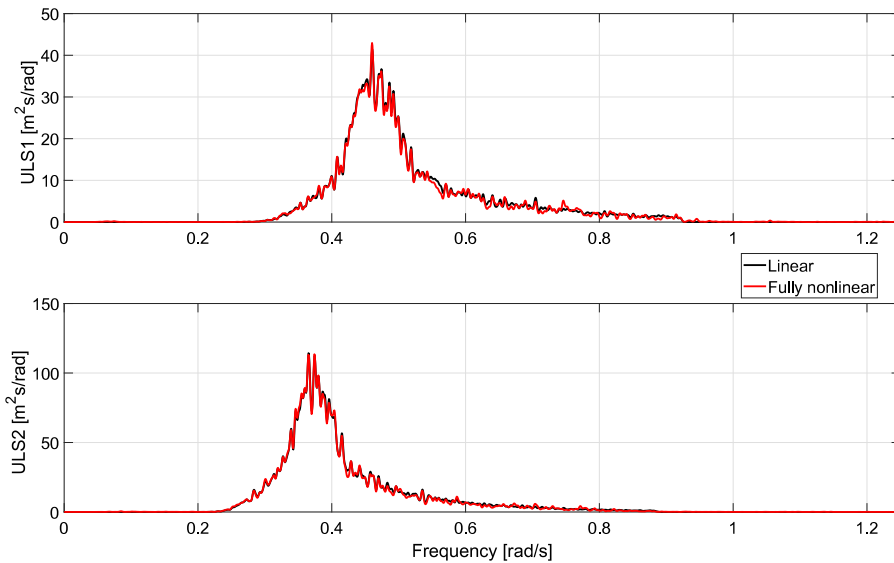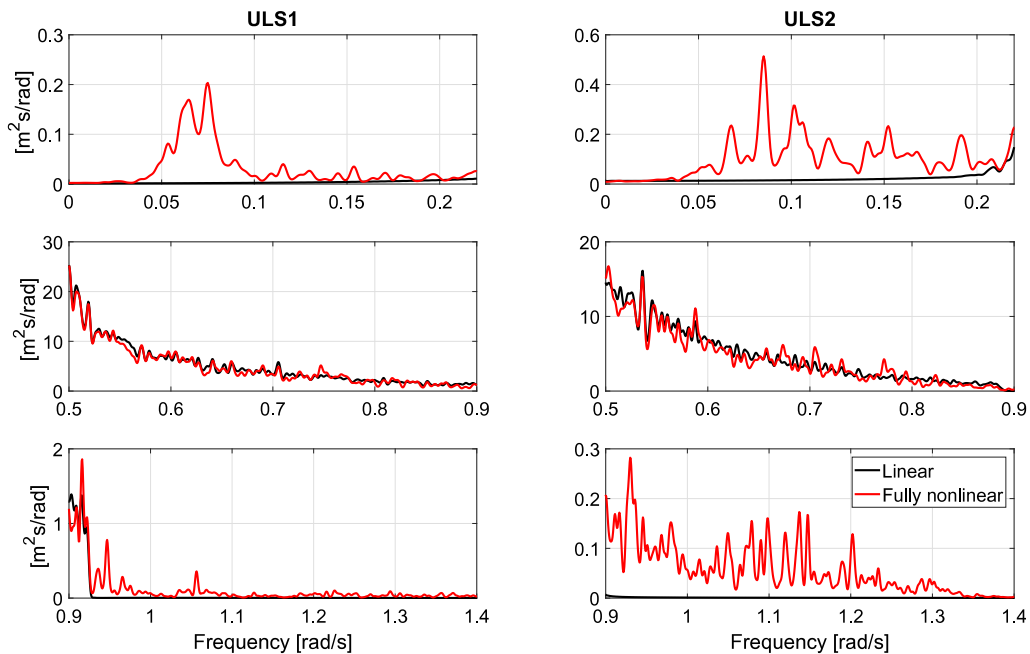
Fig. 21. Wave spectrum.

Fig. 22. Wave spectra at different frequency ranges.

energy than fully nonlinear wave when same random seed is used to generate the wave. Skewness is a measurement of the asymmetry of the maximum and minimum values of a process away from its mean value. The larger the skewness is, the shorter and more peaked the crests of the waves are while the troughs become longer and flatter. In this study, skewness is close to zero for both linear waves which means the peak and trough are equally close to the mean value. Meanwhile, the skewness is larger than zero for nonlinear waves which indicates the asymmetry of the wave profile. Larger kurtosis value for nonlinear wave on the other hand indicates higher nonlinearity than linear wave as expected.

Wave spectrum determines the energy distribution of the wave at different frequencies, which will influence the dynamic response of different natures. The linear and nonlinear spectrum of wave elevation for both cases are compared in Fig. 21. The spectral energy density are calculated for all 20 simulations and the average is used to plot the spectra to get a better representation especially for the low frequency part. The spectra at wave frequency range (ULS1: [0.3 rad/s−1 rad/s] & ULS2: [0.25 rad/s−1 rad/s]) are quite similar for linear and nonlinear wave containing most of the energy. The
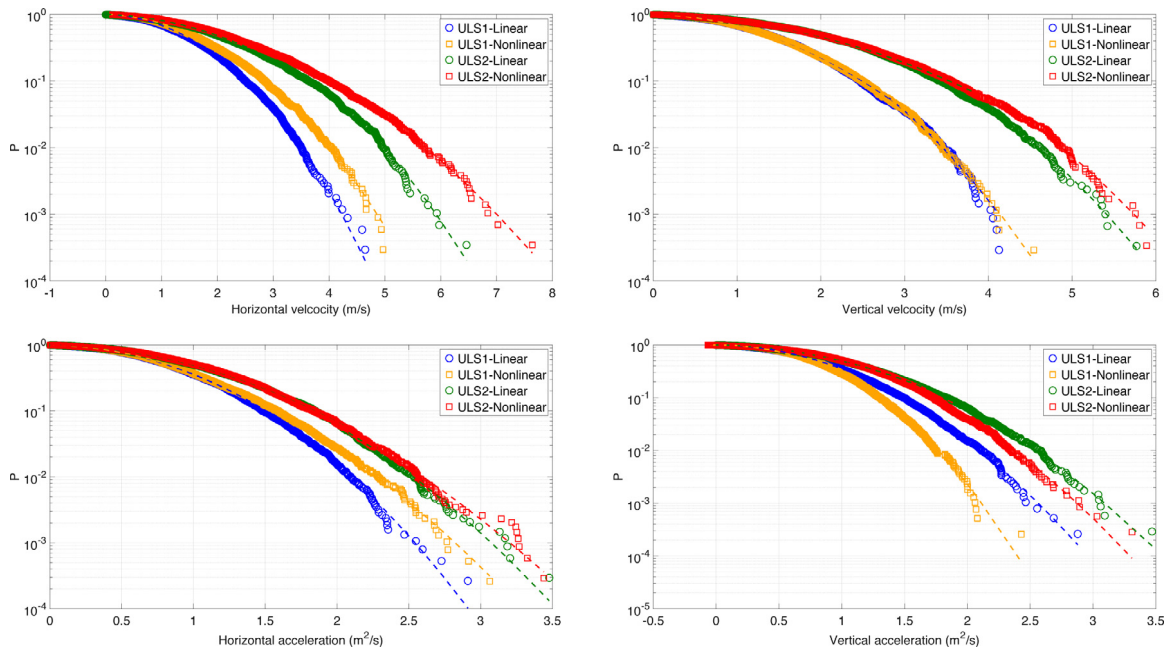
Fig. 23. Global maxima of wave kinematics at instantaneous water level above (0 m, 0 m, 0 m).

main difference is located at higher and lower frequency. The wave spectra are zoomed in at three frequency ranges as shown in Fig. 22. It is seen that linear wave tends to have more energy at range [0.5 rad/s–0.9 rad/s] than nonlinear wave. At the same time, nonlinear wave relocates more energy at higher range [0.9 rad/s–1.4 rad/s] and lower range [0 rad/s–0.2 rad/s]. Initially, the wave spectrum used for generating the irregular wave is the same for linear and fully nonlinear wave and the difference of the energy distribution in the resulting wave spectrum for different frequency range is due to nonlinear free surface effect and contact effect from seabed during wave development. Different responses are directly affected by wave energy distribution at corresponding range, such as surge motion in low frequency range and tower base shear force and bending moment at wave frequency range. The influence will be seen later in the response results.

6.4.3. Wave kinematics

The hydrodynamic wave load in HAWC2 is calculated based on Morison's equation (Eq. (11)) where wave kinematics including wave particle velocity and acceleration are the input variables. Therefore, prediction of the wave kinematics will directly affect the load calculation and further response level. Long-crested wave approximation is the basis of the wave formulation in HAWC2 which means that the wave energy propagates in one direction, i.e. 2D waves. Due to the decay of wave kinematics from free surface to seabed, the global maxima of wave kinematics at instantaneous water level above location (0 m, 0 m, 0 m) is compared in Fig. 23. In horizontal direction, linear wave model predicts smaller value for both velocity and acceleration in both conditions. At the same time, close prediction is seen for vertical velocity while linear wave model estimates higher vertical acceleration than fully nonlinear wave model.

6.4.4. Floater motion

Floater motion of a semi-submersible floating wind turbine is influenced by not only the wave-frequency wave load but also higher-order (low-frequency) wave load to a great extent. The statistics of motion response shown in Table 5 is calculated as the mean of all 20 simulations. Overall, larger motion response is observed at higher sea states as expected in Fig. 24. Little difference is found in heave and pitch motion for all the statistics from the two wave models. However, significant difference is observed for surge motion regarding mean value, maximum value and standard deviation. Linear wave model underestimates both the maximum and standard deviation for surge motion significantly.

The motion response spectra are compared in Fig. 25. For surge motion, little contribution is from wave frequency component while significant contribution is from surge resonance whose natural frequency is located between [0 rad/s–0.2 rad/s] where fully nonlinear wave contains more energy than linear wave due to energy relocation as shown in Fig. 22. Therefore, linear wave underestimates surge response compared with fully nonlinear wave, which is one of the most important findings in this paper. As for heave and pitch motion, both of them are governed by wave frequency response where linear and fully nonlinear wave contains similar energy and very little contribution is due to motion resonance. Therefore almost identical power spectra and statistics are estimated from two wave models.
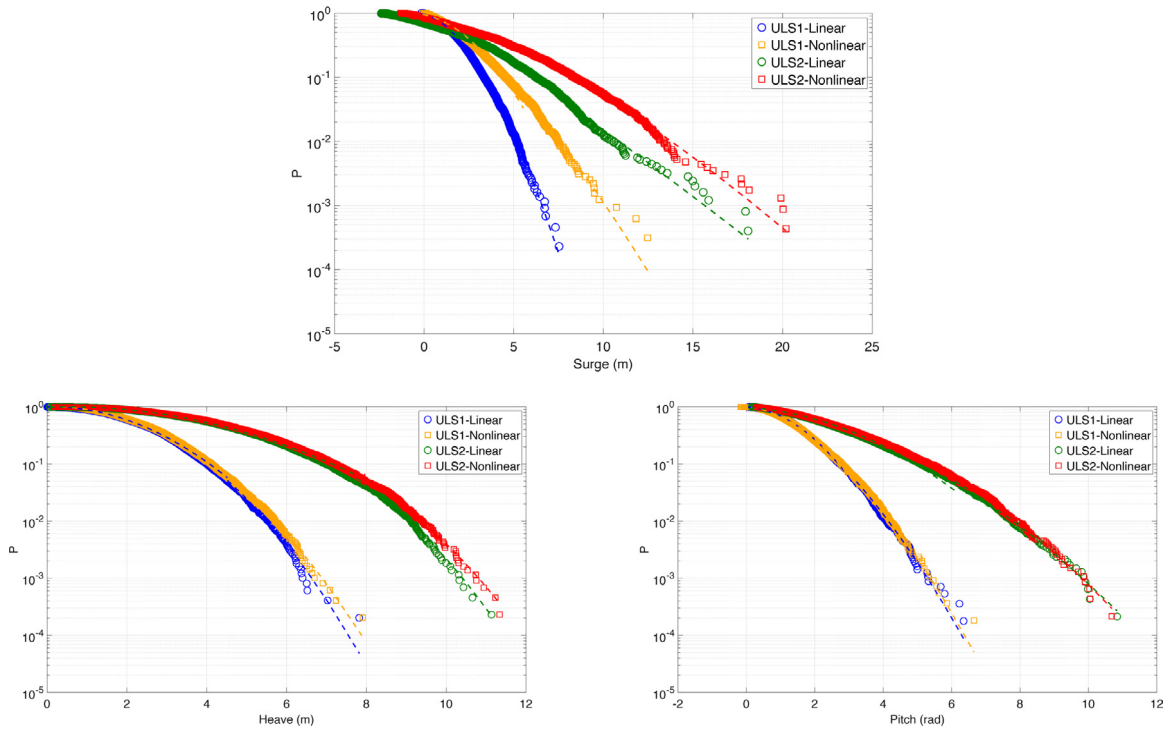
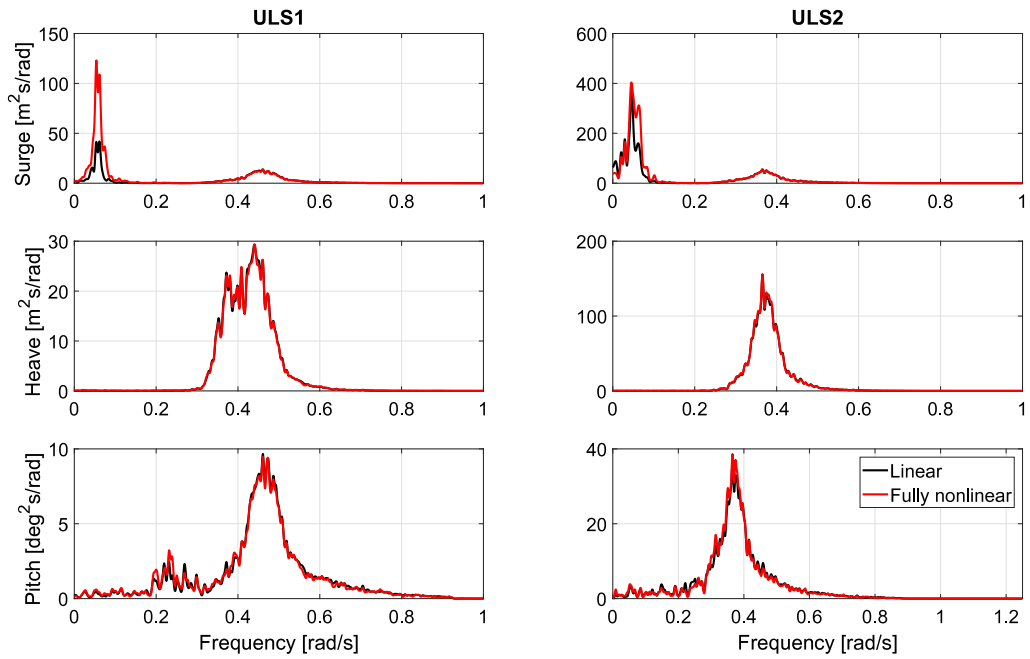**Fig. 24.** Global maxima of floater motions.

**Fig. 25.** Motion spectrum.

6.4.5. Tower base

The shear force and bending moment parallel to incoming wave direction at the tower base are studied in Fig. 26. It is very interesting to notice that both shear force and bending moment predicted from linear wave model are in general

Table 5
Statistics of motion response.

		ULS1 linear	ULS1 nonlinear	ULS2 linear	ULS2 nonlinear
Surge	Mean [m]	0.0981	0.126	0.921	1.96
	Maximum [m]	5.94	8.80	10.2	14.0
	Std [m]	1.56	2.10	4.09	4.41
	Skewness	0.152	0.242	−0.268	−0.0493
	Kurtosis	3.29	3.59	3.09	4.07
	Extreme 10^{-4} [m]	7.99	13.67	23.87	26.74
Heave	Mean [m]	0.0189	0.112	0.0482	0.179
	Maximum [m]	6.21	6.43	9.63	10.0
	Std [m]	1.85	1.84	3.29	3.29
	Skewness	0.0760	0.122	0.0435	0.0931
	Kurtosis	2.73	2.74	2.48	2.48
	Extreme 10^{-4} [m]	7.53	7.81	11.29	11.78
Pitch	Mean [deg]	0.0713	0.0606	0.203	0.295
	Maximum [deg]	5.13	5.10	8.70	8.86
	Std [deg]	1.19	1.18	2.10	2.11
	Skewness	0.249	0.313	0.415	0.519
	Kurtosis	3.35	3.38	3.56	3.51
	Extreme 10^{-4} [deg]	6.58	6.55	11.58	11.33
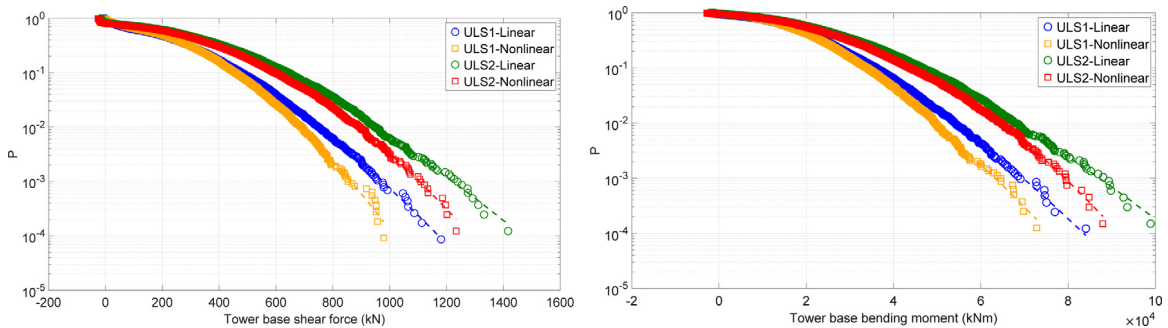
Fig. 26. Global maxima of tower base shear force and bending moment.
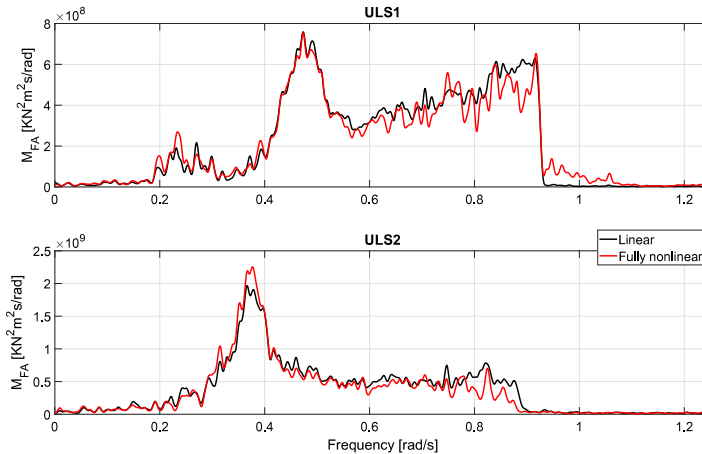
Fig. 27. Tower base bending moment spectrum.

larger than from nonlinear wave model. This is because both of them are mainly influenced by the wave frequency effect where linear wave contains more energy as shown in Fig. 22.

The power spectrum for the bending moment is compared in Fig. 27 for both conditions. More energy is located between [0.6 rad/s–0.9 rad/s] for linear wave which leads to larger response for shear force and bending moment while fully nonlinear transfers more energy to the frequency beyond cut-off limit to which tower base response is not very sensitive to.
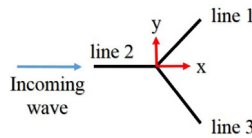
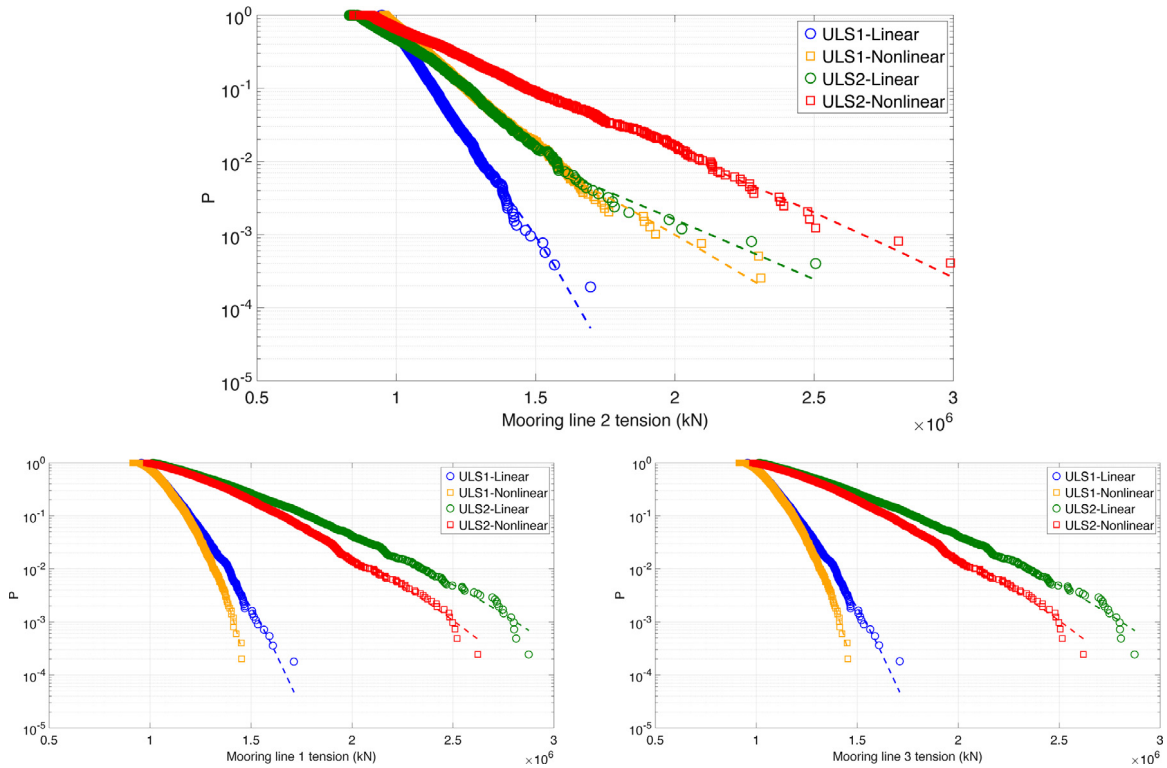**Fig. 28.** Mooring configuration and incoming wave direction.

Fig. 29. Global maxima of mooring line tension.

6.4.6. Mooring line tension

Three mooring lines are equally spaced with angle of 120 degrees between each line as illustrated in Fig. 28 with the numbering. Maximum mooring line tension is located at fairlead which is mainly influenced by motion of the floater. The tension of the two mooring lines (line 1&3) in downwind direction are quite similar with each other. Because linear wave predicts smaller surge motion, the mooring line in downwind direction is relatively less slack than fully nonlinear wave condition which leads to higher tension response predictions. As for the upwind mooring line (line 2), since it faces incoming wave directly, the difference is quite obvious even for smaller sea state and becomes more significant for higher wave condition. The maximum, skewness and kurtosis of the tension response are listed in Table 6.

The maximum tension predicted from linear wave is smaller than from nonlinear wave in ULS1 and ULS2 condition respectively. Higher skewness and kurtosis are found for nonlinear wave model which indicates higher nonlinear and non-Gaussian property of the tension due to effects from nonlinear wave and nonlinear mooring line character. The difference is quite obvious for high sea state. Meanwhile, the combination of Rayleigh and Weibull distribution has been proved to be a really good probability model to predict the probability distribution of the tension response especially regarding the extreme response at the tail part (see Fig. 29).

The power spectrum for mooring line 2 is compared in Fig. 30. Surge resonance dominates the mooring line tension response with additional contribution from wave frequency. The difference from linear and fully nonlinear wave is more significant in the surge resonant range (low frequency range) than wave frequency range.

7. Conclusion

Fully nonlinear wave effects on OC4 semi-submersible floating wind turbine at intermediate water depth has been studied in this paper. An innovative way of dealing with big wave kinematics data is proposed and a complete simulation
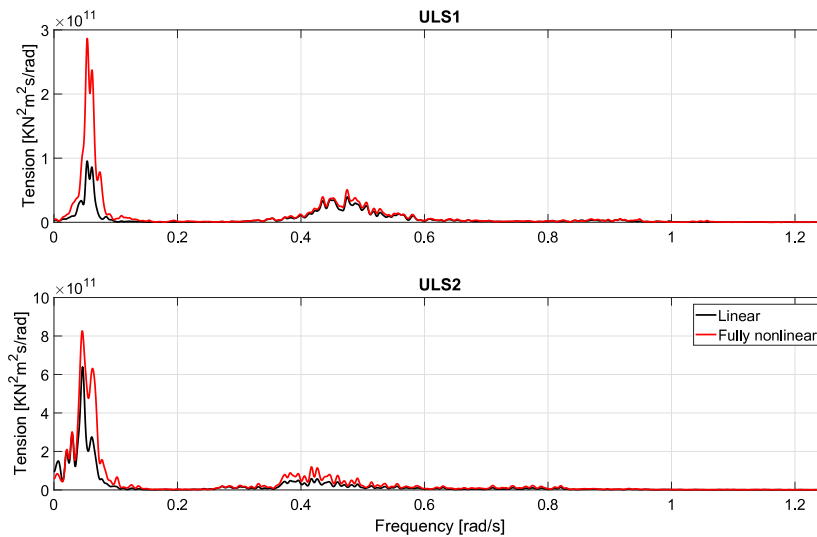
Fig. 30. Mooring line tension spectrum.

Table 6
Statistics of upwind mooring line (Line 2) tension.

	ULS1 linear	ULS1 nonlinear	ULS2 linear	ULS2 nonlinear
Mean [KN]	8.64e+05	9.12e+05	9.48e+05	9.61e+05
Maximum [KN]	1.403e+06	1.758e+06	1.706e+06	2.458e+06
Std [KN]	8.215e+04	1.130e+05	1.687e+05	2.096e+05
Skewness	0.214	1.01	0.743	1.08
Kurtosis	5.31	5.91	6.46	10.1
Extreme 10^{-4} [KN]	1.657e+06	2.438e+06	2.732e+06	3.215e+06

tool is developed which fills the gap in studying fully nonlinear wave effects on floating wind turbine in an engineering way. The comparison of global maxima for the response between linear wave model and fully nonlinear wave model illustrates the importance to consider wave nonlinear effect in hydrodynamic analysis.

In this paper, the linear irregular wave and fully nonlinear irregular wave are generated in 2D HPC numerical wave tank with linear and fully nonlinear free surface boundary conditions respectively. The HPC method once again shows its advantage regarding the accuracy and efficiency in dealing with instantaneous fully nonlinear free surface boundary conditions in time domain. It is able to provide fully nonlinear wave kinematics in an acceptable time without even using super computer.

Due to the configuration of mooring system, the wave field intended for floating wind turbine is much larger than bottom fixed wind turbine which leads to large size of wave kinematics data files. In order to solve the memory barrier of HAWC2 when reading pre-generated wave kinematics file, a polynomial fitting method is proposed to scale down the data size to meet the memory requirement. The wave kinematics is fitted into polynomial functions representing location coordinates associated with polynomial coefficients, which expresses wave kinematics information in a function manner instead of exact value. The fitting polynomial result is checked with original data from wave tank and the accuracy of using the polynomial function in time domain simulation is also verified with a regular wave case study against HAWC2 default wave.

The external dynamic link library used to provide wave kinematics to HAWC2 is extended from one dimensional (Wkin.dll 2.4) to two dimensional (Wkin.dll 2D). The development includes the variation of wave kinematics along horizontal direction which is relevant for floating wind turbine. The fully nonlinear wave kinematics is imported through the extended DLL to HAWC2 in the form of polynomial coefficients. Wkin.dll 2D receives location coordinates from HAWC2 and sends back the exact wave kinematics value for hydrodynamic wave load calculation.

Two irregular wave sea states representing extreme environmental conditions are compared to study fully nonlinear wave effects. Fully nonlinear irregular wave is compared with linear irregular wave generated with same random seed. The wave elevation is clearly underestimated by linear wave model especially for higher sea states. This could be in addition relevant for air gap analysis of offshore oil and gas platform. The different energy distribution is observed from the wave spectrum between linear and nonlinear wave. The nonlinear wave is able to capture contribution from higher and lower range than wave frequency. Comparatively, more energy is relocated by linear wave to the range slightly higher than wave frequency. Higher shear force and bending moment at tower base predicted from linear wave than fully nonlinear wave is a result of this energy distribution. Heave and pitch motion of the floater are predicted quite close with different

wave models since they are mainly wave-frequency load dominating. However, surge motion and mooring line tension which in addition are also greatly influenced by low-frequency wave load is underpredicted using linear wave model. It is well explained by the motion response spectrum with respect to wave spectrum. High nonlinear and non-Gaussian property is captured by nonlinear wave especially when sea states becomes more extreme.

In conclusion, the paper not only proves the importance to include fully nonlinear wave effect in hydrodynamic analysis for floating wind turbine exposed to high sea states in shallow and intermediate water depth but also provides a corresponding engineering practical solution.

Acknowledgment

References

Bai, W., Hannan, M., Ang, K., 2014. Numerical simulation of fully nonlinear wave interaction with submerged structures: Fixed or subjected to constrained motion. J. Fluids Struct. 49, 534–553.

Borg, M., Hansen, A.M., Bredmose, H., 2016. Floating substructure flexibility of large-volume 10 MW offshore wind turbine platforms in dynamic calculations. J. Phys. 753.

Bredmose, H., 2013. Fully nonlinear wave forcing of a TLP wind turbine. Deliverable report 4.21 on INNWIND.EU, DTU.

Carrión, M., Steijl, R., Woodgate, M., Barakos, G., Munduate, X., Gomez-Iradi, S., 2014. Aeroelastic analysis of wind turbines using a tightly coupled CFD–CSD method. J. Fluids Struct. 50, 392–415.

Cummins, W.E., 1962. The impulse response function and ship motions. In: Symposium on Ship Theory. University Hamburg.

DNVGL, 2017. DNV-RP-C205 Environmental Conditions and Environmental Loads.

Engsig-Karup, A.P., Bingham, H.B., Lindberg, O., 2009. An efficient flexible-order model for 3D nonlinear water waves. J. Comput. Phys. 228, 2100–2118.

Faltinsen, O.M., Timokha, A.N., 2009. Sloshing. Cambridge University Press.

Fu, P., Leira, B.J., Myrhaug, D., 2017. Reliability analysis of wake-induced collision of flexible risers. Appl. Ocean Res. 62, 49–56.

Gibson, R., Swan, C., 2006. The evolution of large ocean waves: the role of local and rapid spectral changes. Proc. R. Soc. A 463 (2077), 21–48.

Hansen, M.H., Gaunaa, M., Madsen, H.A., 2004. A Beddoes-Leishman type dynamic stall model in state-space and indicial formulations. Risø National Laboratory.

Jonkman, J.M., 2009. Dynamics of offshore floating wind turbines model development and verification. Wind Energy 12 (5), 459–492.

Kallesøe, B.S., Hansen, A.M., 2011. Dynamic mooring line modeling in hydro-aero-elasticwind turbine simulations. In: The Twenty-First International Offshore and Polar Engineering Conference.

Karimirad, M., Meissonnier, Q., Gao, Z., Moan, T., 2011. Hydroelastic code-to-code comparison for a tension leg spar-type floating wind turbine. Mar. Struct. 24 (4), 412–435.

Kim, B.W., Sung, H.G., Kim, J.H., Hong, S.Y., 2013. Comparison of linear spring and nonlinear FEM methods in dynamic coupled analysis of floating structure and mooring system. J. Fluids Struct. 42, 205–227.

Larsen, T.J., Hansen, A.M., 2007. How 2 HAWC2, the user's manual. Risø National Laboratory.

Larsen, T.J., Kim, T., Schløer, S., Bredmose, H., 2011. Comparisons of wave kinematics models for an offshore wind turbine mounted on a jacket substructure. In: Proceedings European Wind Energy Association (EWEA).

Li, L., Gao, Z., Moan, T., 2015. Joint distribution of environmental condition at five european offshore sites for design of combined wind and wave energy devices. J. Offshore Mech. Arctic Eng. 137.

Liang, H., Faltinsen, O.M., Shao, Y.-L., 2015. Application of a 2D harmonic polynomial cell (HPC) method to singular flows and lifting problems. Appl. Ocean Res. 53, 75–90.

Matha, D., Schlipf, M., Cordle, A., Pereira, R., Jonkman, J., 2011. Challenges in simulation of aerodynamics, hydrodynamics, and mooring-line dynamics of floating offshore wind turbines. In: 21st Offshore and Polar Engineering Conference.

Nematbakhsh, A., Bachynski, E.E., Gao, Z., Moan, T., 2015. Comparison of wave load effects on a TLP wind turbine by using computational fluid dynamics and potential flow theory approaches. J. Appl. Ocean Res. 53, 142–154.

Ning, D., Teng, B., 2007. Numerical simulation of fully nonlinear irregular wave tank in three dimension. Internat. J. Numer. Methods Fluids 53, 1847–1862.

Øye, S., 1996. FLEX4 simulation of wind turbine dynamics. In: Proceedings for the 28th IEA Meeting of Experts Concerning State of the Art of Aero-Elastic Codes for Wind Turbine Calculations.

Pegalajar-Jurado, A., Borg, M., Robertson, A., Jonkman, J., Bredmose, H., 2017. Effect of second-order and fully nonlinear wave kinematics on a tension-leg-platform wind turbine in extreme wave conditions. In: 36th International Conference on Ocean, Offshore and Arctic Engineering.

Robertson, A.N., Jonkman, J.M., Masciola, M.D., Molta, P., Goupee, A.J., Coulling, A.J., Prowell, I., Browning, J., 2013. Summary of conclusions and recommendations drawn from the deepcwind scaled floating offshore wind system test campaign. In: 32nd International Conference on Ocean, Offshore and Arctic Engineering.

Robertson, A., Jonkman, J., Masciola, M., Song, H., Goupee, A., Coulling, A., Luan, C., 2014a. Definition of the Semisubmersible Floating System for Phase II of OC4. NREL technical report.

Robertson, A., Jonkman, J., Vorpahl, F., Popko, W., Qvist, J., Froyd, L., Chen, X., Azcona, J., Uzungoglu, E., Guedes Soares, C., et al., 2014b. Offshore code comparison collaboration continuation within IEA wind task 30: Phase II results regarding a floating semi-submersible wind system. In: Proceeding of 33rd International Conference on Ocean, Offshore and Arctic Engineering, vol. 9B.

Santo, H., Taylor, P., Williamson, C., 2018. On the morison hydrodynamic forces on perforated flat plates in combined steady, low frequency and high frequency motion. J. Fluids Struct. 81, 514–527.

Schløer, S., Bredmose, H., Bingham, H.B., 2011. Irregular wave forces on monopile foundations. Effect af full nonlinearity and bed slope. In: 30th International Conference on Ocean, Offshore and Arctic Engineering, vol. 5. American Society of Mechanical Engineers. pp. 581–588.

Schløer, S., Bredmose, H., Bingham, H.B., 2012. The influence of fully nonlinear wave forces on aero-hydro-elastic calculations of monopile wind turbines. In: Proceedings of the ASME 31st International Conference on Ocean, Offshore and Arctic Engineering, vol. 7. pp. 393–402.

Schløer, S., Bredmose, H., Bingham, H.B., 2016. The influence of fully nonlinear wave forces on aero-hydro-elastic calculations of monopile wind turbines. Mar. Struct. 50, 162–188.

Shao, Y.-L., Faltinsen, O.M., 2012. Towards efficient fully-nonlinear potential-flow solvers in marine hydrodynamics. In: ASME 2012 31st International Conference on Ocean, Offshore and Arctic Engineering. American Society of Mechanical Engineers, pp. 369–380.

Shao, Y.-L., Faltinsen, O.M., 2014a. Fully-nonlinear wave-current-body interaction analysis by a harmonic polynomial cell method. J. Offshore Mech. Arct. Eng. 136 (3), 031301.

Shao, Y.-L., Faltinsen, O.M., 2014b. A harmonic polynomial cell (HPC) method for 3D Laplace equation with application in marine hydrodynamics. J. Comput. Phys. 274, 312–332.

Stansberg, C.T., Gudmestad, O.T., Haver, S.K., 2008. Kinematics under extreme waves. J. Offshore Mech. Arct. Eng. 130 (2), 021010.